HAL
open science

Modulation of Synaptic Plasticity by Glutamatergic Gliotransmission: A Modeling Study

Maurizio de Pittà, Nicolas Brunel

To cite this version:

Maurizio de Pittà, Nicolas Brunel. Modulation of Synaptic Plasticity by Glutamatergic Gliotransmission: A Modeling Study. Neural plasticity, 2016, 10.1155/2016/7607924 . hal-01353306

HAL Id: hal-01353306

https://hal.science/hal-01353306v1

Submitted on 11 Aug 2016

HAL is a multi-disciplinary open access archive for the deposit and dissemination of scientific research documents, whether they are published or not. The documents may come from teaching and research institutions in France or abroad, or from public or private research centers.

L'archive ouverte pluridisciplinaire **HAL**, est destinée au dépôt et à la diffusion de documents scientifiques de niveau recherche, publiés ou non, émanant des établissements d'enseignement et de recherche français ou étrangers, des laboratoires publics ou privés.

Modulation of synaptic plasticity by glutamatergic gliotransmission: A modeling study

Maurizio De Pittà
Department of Neurobiology
The University of Chicago, Chicago, IL 60637, USA
Project-Team BEAGLE, INRIA Rhône-Alpes, 60097 Villeurbanne, France

Nicolas Brunel
Departments of Statistics and Neurobiology
The University of Chicago, Chicago, IL 60637, USA

August 10, 2016

Abstract

Glutamatergic gliotransmission, that is the release of glutamate from perisynaptic astrocyte processes in an activity-dependent manner, has emerged as a potentially crucial signaling pathway for regulation of synaptic plasticity, yet its modes of expression and function in vivo remain unclear. Here, we focus on two experimentally well-identified gliotransmitter patwhays: (i) modulations of synaptic release and (ii) postynaptic slow inward currents mediated by glutamate released from astrocytes, and investigate their possible functional relevance on synaptic plasticity in a biophysical model of an astrocyte-regulated synapse. Our model predicts that both pathways could profoundly affect both short- and long-term plasticity. In particular, activity-dependent glutamate release from astrocytes, could dramatically change spike-timing–dependent plasticity, turning potentiation into depression (and vice versa) for the same protocol.

Abbreviations

AMPAR: α-amino-3-hydroxy-5-methyl-4-isoxazolepropionic acid receptor; AP: action potential; bAP: back-propagating action potential; ER: endoplasmic reticulum; GPCR: G protein-coupled receptor; LTD: long-term depression; LTP: long-term potentiation; mGluR: metabotropic glutamate receptor; NMDA(R): N-methyl-D-aspartate (receptors); PAR1: protease-activated receptor 1; PPR: pair pulse ratio (E)PSC: (excitatory) postsynaptic current; (E)PSP: (excitatory) postsynaptic potential; SIC: slow inward current; SERCA: sarco-endoplasmic recticulum Ca^{2+}/ATPase; STDP: spike-timing–dependent plasticity; VDCC: voltage-dependent calcium channel.

Introduction

In recent years, astrocytes have attracted great interest for their capacity to release neuroactive molecules, among which are neurotransmitters like glutamate, because these molecules could modulate neural activity and lead to a possible role for astrocytes in neural information processing (Volterra and Meldolesi, 2005; Perea and Araque, 2007; Halassa and Haydon, 2010). Indeed, astrocyte-derived neurotransmitters, also called "gliotransmitters" for their astrocytic origin (Bezzi and Volterra, 2001), have been shown to act on neurons and to regulate synaptic transmission and plasticity through a variety of mechanisms (Araque et al., 2014). The binding of receptors located on either pre- or postsynaptic terminals by astrocyte-released glutamate has historically been the first pathway for gliotransmission to be discovered and, arguably, the most studied one experimentally for its several possible functional implications (Santello and Volterra, 2009).

Activation of extrasynaptic receptors on presynaptic terminals by astrocytic glutamate modulates the probability of neurotransmitter release from those terminals (Santello and Volterra, 2009). In particular, depending on receptor type, such modulation may be either toward an increase or toward a decrease of the frequency of spontaneous (Fiacco and McCarthy, 2004; Jourdain et al., 2007; Bonansco et al., 2011; Panatier et al., 2011; Perea et al., 2014) and evoked neurotransmitter release both in excitatory (Jourdain et al., 2007; Perea and Araque, 2007; Navarrete and Araque, 2010; Panatier et al., 2011) and inhibitory synapses (Liu et al., 2004b,a; Benedetti et al., 2011). Because synaptic release probability characterizes how a synapse filters or, in other words, "processes" presynaptic action potentials (Markram et al., 1998b; Abbott and Regehr, 2004), modulations of synaptic release probability by astrocytic glutamate are suggested to alter the computational properties of neural circuits (De Pittà et al., 2015).

Glutamate released by astrocytes may also bind to extrasynaptically-located postsynaptic NMDA receptors, evoking slow inward currents (SICs) in nearby neurons (Parri et al., 2001; Angulo et al., 2004; Fellin et al., 2004; Perea and Araque, 2005; D'Ascenzo et al., 2007; Shigetomi et al., 2008; Bardoni et al., 2010; Perea et al., 2014; Martín et al., 2015). The depolarizing action of these currents modulates neural excitability with the potential to affect neuronal action potential firing (Halassa et al., 2007a). Moreover, because single astrocytes are in close proximity to a large number ($\sim$100) of neurons (Halassa et al., 2007b), it has been suggested that an inward current can be generated in many adjacent neurons, thereby promoting synchrony of neuronal firing (Parri et al., 2001; Angulo et al., 2004; Fellin et al., 2004).

Although modulations of both synaptic release and SICs mediated by glutamatergic gliotransmission have been recorded in the cortex and the hippocampus, as well as in several other brain regions (Araque et al., 2014), their physiological relevance remains elusive. In particular, beyond regulation of synaptic filtering and neuronal firing, theoretical arguments support a further possible role for both pathways in the regulation of NMDAR-mediated spike-timing–dependent plasticity (STDP) (De Pittà et al., 2013). Both pathways clearly have the potential to regulate activation of postsynaptic NMDA receptors: the former does so indirectly, by modulations of the amount of synaptically-released neurotransmitter molecules that bind to NMDA receptors in the synaptic cleft; the latter directly, by targeting extrasynaptic NMDA receptors. Thus, by controlling postsynaptic NMDAR activation, glutamatergic gliotransmission could ultimately regulate the STDP outcome, that is either potentiation (LTP) or depression (LTD) (Mizuno et al., 2001; Nevian and Sakmann, 2006). Consistent with this hypothesis, experiments have reported a lower threshold for LTP induction at hippocampal synapses when synaptic release is increased by astrocytic glutamate (Bonansco et al., 2011). And long-term potentiation of orientation-selective responses of neurons in the primary visual cortex by cholinergic activation of surrounding astrocytes, has also been reported to be correlated with an increase of SIC

frequency in those neurons (Chen et al., 2012).

While the potential impact on STDP of pre- or postsynaptic activity-dependent modulations of synaptic efficacy have widely been addressed both experimentally (Sjöström et al., 2008) and theoretically (Froemke et al., 2010; Graupner and Brunel, 2010), the possible effect on plasticity of the regulation of these modulations by glutamatergic gliotransmission (and by gliotransmission in general) has been investigated by very few theoretical studies. These studies suggest a potential role in LTP induction both for large increases of synaptic release and for large SICs mediated by astrocytic glutamate (Wade et al., 2011; Naeem et al., 2015). This scenario seems however at odds with the majority of recent experimental observations that report modest signaling magnitudes for these two routes of gliotransmission. It is thus not clear under what biophysical conditions, modulations of synaptic release or SICs mediated by glutamatergic gliotransmission could affect STDP. Astrocyte-mediated SICs, for example, are known to occur sporadically, being recorded in single neurons only as often as <5/min (Chen et al., 2012; Martín et al., 2015), raising the question whether and how, by occurring at such low rates, they could effectively play a role in STDP.

We thus set to investigate what conditions are required for glutamatergic gliotransmission to affect STDP by presynaptic modulations of neurotransmitter release or through postsynaptic SICs. We extend the model of an astrocyte-regulated synapse originally introduced by De Pittà et al. (2011) to include a biophysically-realistic description of synaptically-evoked gliotransmitter release by the astrocyte as well as a mechanism for the generation of postsynaptic SICs and STDP. Extensive numerical investigations of our model leads to two major predictions. First, glutamatergic gliotransmission could change the nature of STDP by modifying the parameter ranges for LTP and LTD induction. Second, this effect crucially depends on the nature of gliotransmission, i.e. whether it is release-increasing vs. release-decreasing, its strength, as well as its rate of occurrence and when it occurs with respect to pre/post pairs. Thus, while glutamatergic gliotransmission could potentially play a role in STDP and learning, in practice this effect must satisfy several biophysical and activity-dependent constraints, supporting the existence of specialized dynamic interactions between astrocytes and neurons.

Biophysical modelling of a gliotransmitter-regulated synapse

Although there may be several possible routes by which astrocytes release glutamate (Ni et al., 2007; Parpura and Zorec, 2010; Zorec et al., 2012), Ca^{2+}-dependent glutamate release is likely the main one in physiological conditions (Barres, 2008; Parpura et al., 2011). From a modeling perspective, as illustrated in Figure 1, Ca^{2+}-dependent glutamatergic gliotransmission consists of three distinct signaling pathways. One pathway (*black arrows*) initiates the release-triggering Ca^{2+} signal in the astrocyte, and may be either exogenous or heterosynaptic, or be triggered by the very synapses that are modulated by glutamatergic gliotransmission in a homosynaptic fashion. The other two pathways are instead represented by the two recognized routes for the action of glutamatergic gliotransmission on synaptic terminals: the presynaptic pathway whereby astrocytic glutamate modulates synaptic release (*magenta arrows*), and the postsynaptic pathway which mediates SICs in nearby neurons (*orange arrows*). Although both pathways could coexist at the same synapse in principle (Perea et al., 2014), their functional regulation is probably through different Ca^{2+}-dependent pathways (Martín et al., 2015), both in terms of spatiotemporal Ca^{2+}-dynamics (Shigetomi et al., 2008) and in terms of pools of releasable glutamate resources and/or mechanism of release for these latter (Hamilton and Attwell, 2010). Thus, in the following, we set to investigate the effect of synaptic transmission of each pathway independently of the other.

Calcium-dependent gliotransmitter release

We begin our study by a description of a biophysically realistic model of synaptically-evoked Ca^{2+}-dependent glutamate release from an astrocyte. At excitatory (Perea et al., 2009) and inhibitory synapses (Losi et al., 2014), astrocytes can respond to synaptically-released neurotransmitters, by intracellular Ca^{2+} elevations and release glutamate in turn (Santello and Volterra, 2009). Although morphological and functional details of the coupling between synaptic terminals and the surrounding astrocytic processes remain to be fully elucidated, the current hypothesis is that synaptically-evoked glutamate-releasing astrocytic Ca^{2+} signaling is mainly by spillover of synaptic neurotransmitters and/or other factors, which bind to high-affinity astrocytic G protein-coupled receptors (GPCRs) (Araque et al., 2014) and thereby trigger inositol 1,4,5-trisphosphate (IP_3) production and Ca^{2+} release from the endoplasmic reticulum (ER) (Nimmerjahn, 2009; Volterra et al., 2014; Bazargani and Attwell, 2016). While early work mainly monitored somatic Ca^{2+} increases concluding that astrocytes respond only to intense neuronal firing patterns (Haydon, 2001), recent experiments in astrocytic processes revealed that astrocytes may also respond to low levels of synaptic activity by Ca^{2+} elevations confined in subcellular regions of their processes (Di Castro et al., 2011; Panatier et al., 2011; Bazargani and Attwell, 2016), suggesting that the profile of astrocytic Ca^{2+} signaling, and thus glutamate release that this latter could cause, encompass the whole spectrum of neuronal (synaptic) activity (Araque et al., 2014).

To realistically describe synaptic release in the whole spectrum of neuronal firing, we consider the model of an activity-dependent synapse first introduced by Tsodyks and Markram (1997). This model captures the dependence of synaptic release on past activity – that is presynaptic short-term plasticity – which substantially influences synaptic transmission at high enough rates of neuronal firing (Zucker and Regehr, 2002). Accordingly, synaptic release results from the product of the probability of having neurotransmitter-containing vesicles available for release times the probability of such vesicles to be effectively released by an action potential (Del Castillo and Katz, 1954), which correlates with intrasynaptic Ca^{2+} (Südhof, 2004). At rest, it is assumed that all vesicles are available for release. The arrival of an action potential opens presynaptic voltage-dependent Ca^{2+} channels that trigger a transient increase of intrasynaptic Ca^{2+} which promotes release of a fraction u_S of available vesicles. Following release, the emptied vesicles are refilled in some characteristic time τ_d, while intrasynaptic Ca^{2+}, and thus vesicle release probability, decay to zero with a different time constant τ_f. For multiple action potentials incoming at time intervals of the order of these two time constants, neither vesicle replenishment nor intrasynaptic Ca^{2+} are restored to their resting values, so that the resulting synaptic release depends on the history of synaptic activity (Tsodyks, 2005).

We illustrate the response of the synapse model to a train of action potentials in Figures 2A–C. The low rate of stimulation of the first four action potentials (Figure 2A) allows for the reintegration of most of the released neurotransmitter in between action potentials thereby keeping vesicle depletion limited (Figure 2B, *orange trace*). In parallel, intrasynaptic Ca^{2+} grows, and so does vesicle release probability (Figure 2B, *blue trace*), resulting in progressively larger release of neurotransmitter per action potential or, in other words, in short-term facilitation of synaptic release (Figure 2C, $t < 500$ ms). On the contrary, the presentation of a series of action potentials in rapid succession at $t = 500$ ms, results in a sharp increase of vesicle release probability to a value close to saturation (i.e. Nt. Rel. Pr.$\simeq 1$) which causes exhaustion of neurotransmitter resources (i.e. Avail. Nt. Pr.$\simeq 0$). In this scenario therefore, from one spike to the next one, progressively less neurotransmitter is available for release and the amount of released resources decreases with incoming action potentials, leading to depression of synaptic transmission. Such depression is short-lived, since synaptic release tends to recover after a suf-

ficiently long period in which no action potentials occur, that is the case, for example, of the last action potential at $t = 800$ ms.

Once released into the synaptic cleft, synaptic neurotransmitter is rapidly cleared by diffusion as well as by other mechanisms, including uptake by transporters and/or enzymatic degradation (Clements, 1996; Diamond, 2005). In the simplest approximation, the contribution of these mechanisms can be modeled by a first order reaction (Destexhe et al., 1994) which accounts for the exponentially decaying profile of neurotransmitter concentration in Figure 2C after synaptic release at each action potential. A fraction of released neurotransmitter molecules also spills out of the synaptic cleft to the perisynaptic space (Figure 2D) where it binds to GPCRs on the astrocyte (Figure 2E), therein triggering Ca^{2+} signaling (Figure 2F). To quantitatively describe this process, we modify the model of GPCR-mediated Ca^{2+} signaling originally introduced by De Pittà et al. (2009a) to account for dynamic regulation of astrocytic receptors by synaptic activity (see Appendix A, Section A.1). Accordingly, as illustrated in Figure 2F, GPCR-mediated Ca^{2+} signaling is a result of the nonlinear interplay of three processes: (i) IP_3 production by GPCRs bound by synaptic neurotransmitter (*magenta trace*), (ii) Ca^{2+} release from the ER into the cytosol, which is triggered by IP_3-bound Ca^{2+} channels (IP_3Rs) and also modulates cytosolic IP_3 (*black trace*); and (iii) the effective fraction of available, or more exactly, "deinactivated" IP_3Rs (De Young and Keizer, 1992) that can take part in Ca^{2+} release from the ER (*yellow trace*). Depending on the choice of parameter values, the astrocyte model may display both large, long-lasting somatic Ca^{2+} elevations, and smaller and shorter Ca^{2+} increases, akin to those reported in astrocytic processes (Volterra et al., 2014) (see Appendix B).

Glutamate release from the astrocyte is then assumed to occur every time that Ca^{2+} increases beyond a threshold concentration (Figure 2G, *cyan dotted line*), in agreement with experimental observations (Pasti et al., 1997; Marchaland et al., 2008). Although different mechanisms for glutamate release by the astrocyte could be possible, a large amount of evidence points to vesicular exocytosis as the main one to likely occur on a physiological basis (Sahlender et al., 2014). Because astrocytic glutamate exocytosis bears several similarities with its synaptic homologous (reviewed in De Pittà et al. (2013)), we model it in the same fashion. Thus, in line with experimental observations (Bezzi et al., 2004; Bergersen and Gundersen, 2009), we postulate the existence of an astrocytic vesicular compartment that is competent for regulated glutamate exocytosis. Then, upon a suprathreshold Ca^{2+} elevation, a fixed fraction of astrocytic glutamate-containing vesicles is released into the extracellular space and following reintegrated into the astrocyte with some characteristic time constant (Figure 2H). In this fashion, glutamate concentration in the extracellular space abruptly increases by exocytosis from the astrocyte, and then exponentially decays akin to neurotransmitter concentration in the synaptic cleft, yet, in general, at a different rate (Figure 2H) (Appendix B).

The description of gliotransmitter release hitherto introduced ignores the possible stochastic nature of astrocytic glutamate release (Santello et al., 2011), and reproduces the total amount of glutamate released, on *average*, by a single Ca^{2+} elevation beyond the release threshold. This description provides a simplified general framework to realistically capture synaptically-evoked glutamate release by the astrocyte independently of the underlying mechanism of astrocytic exocytosis, which may either be in the form of a burst of synchronous vesicle fusion events that peaks within the first 50–500 ms from the Ca^{2+} rise underneath the plasma membrane (Domercq et al., 2006; Marchaland et al., 2008; Santello et al., 2011), or occur at slower fusion rates in an asynchronous fashion (Kreft et al., 2004; Malarkey and Parpura, 2011).

Gliotransmitter-mediated regulation of synaptic release and short-term synaptic plasticity

Once released, astrocyte-derived glutamate can diffuse in the extracellular space and bind extrasynaptic receptors located on presynaptic terminals. In particular, ultrastructural evidence suggest co-localization of glutamate-containing vesicles in perisynaptic astrocytic processes with those receptors (Jourdain et al., 2007), hinting a focal action of astrocytic glutamate on these latter. Such action is likely spatially confined and temporally precise, akin to that of a neurotransmitter on postsynaptic receptors, and is not affected by synaptic neurotransmitters (Santello and Volterra, 2009). Both ionotropic and metabotropic presynaptic receptors may be activated by astrocytic glutamate, yet their differential recruitment likely depends on developmental, regional, physiological and cellular (synaptic) factors (reviewed in (De Pittà et al., 2013)). The details of the biochemical mechanisms of action of these receptors on synaptic physiology are not fully understood (Pinheiro and Mulle, 2008), but the simplest explanation is that they all modulate intrasynaptic Ca^{2+} levels eventually increasing or decreasing synaptic release probability (De Pittà et al., 2015), although in a receptor-specific fashion (Zucker and Regehr, 2002; Pinheiro and Mulle, 2008; Banerjee et al., 2015).

From a modeling perspective, as originally proposed by De Pittà et al. (2011), the common effect on synaptic release shared by different receptors allows to express, in the simplest approximation, the synapse's resting release probability proportionally to the fraction of presynaptic receptors activated by astrocytic glutamate (Appendix A, Section A.1). In this fashion, as illustrated in Figure 3, the time evolution of the fraction of activated presynaptic receptors ensuing from a series of glutamate release events by the astrocyte (Figures 3A,B), is reflected by the dynamics of synaptic release probability at rest averaged across different trials (Figures 3C,E). The value of the coefficient of proportionality for the dependence of synaptic release probability on receptor activation sets the type of modulation of synaptic release by astrocytic glutamate which can be either release-decreasing (Figure 3C), such as in the case of astrocytic glutamate binding presynaptic kainate receptors or group II/III metabotropic receptors (mGluRs) (Araque et al., 1998a; Liu et al., 2004b,a), or release-increasing (Figure 3E), when astrocytic glutamate binds NMDARs or group I mGluRs (Fiacco and McCarthy, 2004; Jourdain et al., 2007; Navarrete and Araque, 2010; Bonansco et al., 2011; Navarrete et al., 2012a; Perea et al., 2014; Martín et al., 2015). The functional implications of these modulations of synaptic release by glutamatergic gliotransmission on synaptic transmission have been widely addressed in a series of previous studies (De Pittà et al., 2011, 2013; De Pittà et al., 2015), and the remainder of this section reviews and extends the main results from those studies about short-term synaptic plastic and synaptic filtering.

Figure 3D (*left panel*) shows how postsynaptic currents (PSCs) change in the presence of release-decreasing glutamatergic gliotransmission when elicited by two consecutive action potentials arriving to the resting synapse 20 ms after the onset of gliotransmission at $t = 5$ s (Figure 3C). Two differences with respect to the case without gliotransmission (*black trace*) may be observed. First the PSC amplitude overall decreases (*red trace*), consistent with a decrease of synaptic efficacy caused by the reduction of synaptic release by astrocytic glutamate. Then, the second PSC is larger then the first one, which is the opposite of what would be measured in the absence of gliotransmission. In other words, in agreement with experimental observations (Liu et al., 2004b), the release-decreasing effect of astrocytic glutamate results in an increased pair pulse ratio (PPR) with respect to the case without gliotransmission (PPR_0). Notably, as shown in Figure 3D (*right panel*), this change in the PPR ratio is only transient and vanishes together with the effect of gliotransmission on synaptic release. Similar considerations also hold in the case of a release-increasing effect of astrocytic glutamate on synaptic transmission (Jourdain

et al., 2007): while PSC amplitude increases (Figure 3F, *left panel*, *green trace*), this occurs to the detriment of PPR, which decreases instead (Figure 3F, *right panel*). Thus, synapses whose release probability is increased by glutamatergic gliotransmission are likely to run out faster of neurotransmitter, exhibiting rapid onset of short-term depression, consistent with lower PPR values. On the contrary, synapses whose release probability is reduced by astrocyte-released glutamate, deplete their neurotransmitter resources slower and may exhibit progressive facilitation (i.e. potentiation) of their efficacy to transmit action potentials, and so larger PPR values (Dittman et al., 2000). That is, the plasticity mode of a synapse, namely whether it is depressing or facilitating, may not be fixed but rather be modulated by glutamatergic gliotransmission by surrounding astrocytes in an activity-dependent fashion (De Pittà et al., 2011, 2013).

An important consequence of short-term synaptic dynamics is that synapses can act as filters (Markram et al., 1998b; Fortune and Rose, 2001; Abbott and Regehr, 2004). Hence, modulations of synaptic dynamics by glutamatergic gliotransmission are also expected to affect the synapse's filtering characteristics (De Pittà et al., 2015). This scenario is illustrated in Figure 4 where the effect of release-decreasing vs. release-increasing glutamatergic gliotransmission, respectively on depressing and facilitating synapses, is shown in terms of changes of the filtering characteristics of these synapses, i.e. their steady-state release as function of the frequency of presynaptic stimulation (Abbott and Regehr, 2004). In the absence of gliotransmission, depressing synapses, which are characterized by intermediate-to-high initial probability of release (Dittman et al., 2000) (Figure 4A, *black circles*), predominantly act as low-pass filters (Figure 4B, *black circles*) that are most effective at transmitting low frequency pre-synaptic spike trains (Figure 4C, *black traces*). On the contrary, facilitating synapses, with a low-to-intermediate initial probability of neurotransmitter release (Dittman et al., 2000) (Figure 4A, *black circles*), function as high-pass or band-pass filters (Figure 4B, *black circles*), that is they are mostly effective at transmitting action potentials in an intermediate range of presynaptic activity (Figure 4C, *black trace*).

In the presence of glutamate release by the astrocyte, these two scenarios could be reversed. Consider indeed the simple heterosynaptic case where glutamatergic gliotransmission is stimulated by other means than by the very synapses it impinges on. It may be noted that release-decreasing gliotransmission flattens the synaptic steady-state release towards zero for all frequencies of stimulation (Figure 4B, *red circles*), ensuing in synaptic transmission that resembles the one of a facilitating, band-pass synapse (compare the *red* PSC *trace* in Figure 4C with the *black* PSC *trace* in Figure 4F). Vice versa, release-increasing gliotransmission could turn band-pass features of transmission by a facilitating synapse (Figure 4E, *green circles*) into low-pass, reminiscent of a more depressing synapse (compare the *green* PSC *trace* in Figure 4F with the *black* PSC *trace* in Figure 4C). On the other hand, when gliotransmission is stimulated by the same synapses that it modulates – that is, in the homosynaptic scenario of gliotransmission –, inspection of the ensuing synaptic filtering characteristics (Figure 4B,E, *cyan circles*) reveals that these latter coincide with those obtained in the absence of gliotransmission for low frequencies of presynaptic activity, while they tend to equal those observed with heterosynaptic gliotransmission as the frequency of stimulation increases. This coexistence of mixed features from apparently opposite scenarios, i.e. no gliotransmission vs. heterosynaptic gliotransmission, can be explained by the fact that the release of glutamate from the astrocyte requires intracellular Ca^{2+} to cross a threshold concentration. Hence, in the homosynaptic scenario, synapses that impinge on the astrocyte must be stimulated at rate sufficiently high to allow astrocytic Ca^{2+} to increase beyond such a threshold.

The modulation of synaptic filtering by glutamatergic gliotransmission opens to the possiblity that the same stimulus could be differently filtered (i.e. processed) and transmitted by a synapse in the presence (or not) of glutamate release by surrounding astrocytic processes,

ultimately endowing that synapse with processing versatility with respect to incoming action potentials. Moreover, to the extent that synaptic dynamics critically shapes the computations performed by the neural circuitry, such versatility could also be reflected at the network level, leading to the possibility that the same neuron-glia network could be involved in different computational tasks defined, time by time, by activity-dependent gliotransmitter release by astrocytes in the network.

Astrocyte-mediated slow inward currents

Induction of slow inward (i.e. depolarizing) currents (SICs) by activation of extrasynaptically-located postsynaptic NMDA receptors is the other mechanism considered in this study whereby glutamatergic gliotransmission could affect synaptic information transfer. While astrocyte-mediated SICs have been reported in several brain regions, the pathway underlying glutamate release by astrocytes has not been fully elucidated (Agulhon et al., 2008; Papouin and Oliet, 2014). It is likely that, similar to the presynaptic route for glutamatergic gliotransmission discussed above, multiple pathways for glutamate release could be used by the same astrocyte (Parpura and Zorec, 2010), but their deployment depends on developmental, regional and physiological factors (Halassa et al., 2007a). Astrocytic Ca^{2+} activity seems a crucial factor in the regulation of astrocyte-mediated SICs (Parri et al., 2001; Angulo et al., 2004; Fellin et al., 2004; Perea and Araque, 2005; D'Ascenzo et al., 2007; Bardoni et al., 2010; Pirttimaki et al., 2011). In particular, SIC frequency and amplitude have been shown to increase upon Ca^{2+} elevations mediated by GPCRs on astrocytes such as mGluRs (Parri et al., 2001; Angulo et al., 2004; Fellin et al., 2004; Perea and Araque, 2005; D'Ascenzo et al., 2007; Navarrete et al., 2012b,a), the metabotropic purinergic P2Y1 receptor (Bardoni et al., 2010), the endocannabinoid CB1 receptor (Navarrete and Araque, 2008) or the protease-activated receptor 1 (PAR1) (Shigetomi et al., 2008). Remarkably, stimulation of PAR1s on hippocampal astrocytes was shown to trigger, under physiological conditions, Ca^{2+}-dependent glutamate release from these cells through Bestrophin-1 anion channel (Oh et al., 2012; Woo et al., 2012), and this pathway of glutamate release has been suggested as a candidate mechanism for SICs (Papouin et al., 2012). Channel-mediated glutamate release is expected to account for prolonged (>10 s) release of transmitter but in small amounts per unit time (Woo et al., 2012) thus ensuing in modest, very slow rising and decaying inward currents. While similar SICs have indeed been recorded (Araque et al., 1998a; Lee et al., 2007), most experiments reported SICs within a wide range of amplitudes to last only few seconds at most and, rise in correlation with astrocytic Ca^{2+} increases with rise time much shorter than their decay (Fellin et al., 2004; Angulo et al., 2004; Perea and Araque, 2005; Shigetomi et al., 2008; Nie et al., 2010; Reyes-Haro et al., 2010; Chen et al., 2012; Martín et al., 2015) akin to currents that would ensue from a quantal mechanism of gliotransmitter release (Sahlender et al., 2014).

Based on these arguments, we assume glutamate exocytosis as the candidate mechanism for glutamate release by astrocytes that mediates SICs. Accordingly, we adopt the description of astrocytic glutamate exocytosis previously introduced (Figures 2G–I) to also model astrocyte-mediated SICs. In this fashion, glutamate exocytosis by the astrocyte into the extracellular space (Figure 5A) results in activation of extrasynaptically-located NMDARs on nearby neuronal dendrites which trigger SICs (Figure 5B) that cause slow depolarizing postsynaptic potentials (PSP, Figure 5C).

An important functional consequence of SIC-mediated depolarizations, is that they can modulate neuronal excitability (Fellin et al., 2004; Perea and Araque, 2005; D'Ascenzo et al., 2007; Nie et al., 2010). As illustrated in Figures 5D,E, astrocyte-mediated SICs (*cyan trace*) may add to regular synaptic currents (*black trace*) resulting in depolarizations of postsynaptic

neurons closer to their firing threshold (D'Ascenzo et al., 2007). In turn, these larger depolarizations could dramatically change generation and timing of action potentials by those neurons in response to incoming synaptic stimuli (Figure 5F). This could ultimately affect several neurons within the reach of glutamate released by an astrocyte, leading to synchronous transient increases of their firing activity (Fellin et al., 2004). Remarkably, this concerted increase of neuronal excitability has often been observed in correspondence with large amplitude (i.e. >100 pA) SICs (Fellin et al., 2004; Kang et al., 2005; Bardoni et al., 2010; Nie et al., 2010), but experiments report the majority of SICs to be generally smaller, with amplitudes <80 pA (Fellin et al., 2004; Kang et al., 2005; Perea and Araque, 2005; Chen et al., 2012; Perea et al., 2014; Martín et al., 2015). It is therefore unclear whether SIC-mediate increase of neuronal excitability could occur (Fellin et al., 2006) or not (Kang et al., 2005; Tian et al., 2005; Ding et al., 2007) in physiological conditions.

In Figure 5G, we consider postsynaptic firing in a standard leaky integrate and fire neuron model (Fourcaud and Brunel, 2002; Burkitt, 2006) as a function of presynaptic activity for SICs of different amplitudes (30–45 pA, see Appendix B) randomly occurring at an average rate of 1 Hz based on a binomial process for glutamate release from astrocytes as suggested by experiments (Santello et al., 2011) (see Appendix A). In line with experimental evidence (Rauch et al., 2003), the input-output transfer function in the absence of gliotransmission has a typical sigmoidal shape (*black dots*) which reflects: (i) gradual emergence of firing for low (>10 Hz) fluctuating synaptic inputs; (ii) the progressive, quasi-linear increase of the firing rate for presynaptic activity beyond ∼30 Hz; and finally, (iii) saturation of the firing rate for sufficiently strong synaptic inputs such that timing of action potential generation approaches the neuron's refractory period (which was fixed at 2 ms in the simulations, Appendix B) (Burkitt, 2006). The addition of astrocyte-mediated SICs alters the firing characteristics of the neuron due to the ensuing larger depolarization. In particular the neuron could generate action potentials for lower rates of presynaptic activity (*cyan/blue dots*). Clearly, the larger the SIC is, the more postsynaptic firing increases with respect to the case without SICs, for a given level of presynaptic activity.

As previously mentioned, these results assume an average 1 Hz rate for astrocyte-mediated SICs. While this is possible in principle, it seems unlikely as following explained. The weak correlation of SIC amplitude with somatic Ca^{2+} elevations observed in experiments favors indeed the idea that glutamate-mediate SICs are highly localized events, occurring within subcellular domains at astrocytic processes (Perea and Araque, 2005). In turn, Ca^{2+}-elevations in astrocytic processes could be as short-lived as ∼0.5 s (Di Castro et al., 2011; Panatier et al., 2011), thus in principle allowing for glutamate release rates of the order of 1 Hz. However, in practice, reported SIC frequency are much lower, that is <5/min (i.e. ∼0.08 Hz) (Perea and Araque, 2005; Perea et al., 2014). Hence, it may be expected that the effect of SICs on neuronal firing could be considerably reduced with respect to the case considered in Figure 5G.

We consider this possibility more closely in Figure 5H, where we analyze postsynaptic firing in function of the average frequency of astrocyte-mediated SICs, both in the absence of synaptic activity (*black* and *dark blue dots*), and in the case of presynaptic activity at an average rate ∼1 Hz, which corresponds to typical levels of spontaneous activity in vivo (Hromádka et al., 2008) (*grey* and *light blue dots*). It may be noted that the effect of SICs of typical amplitudes on postsynaptic firing rate is generally small, i.e. <0.5 Hz, except for unrealistic (>0.1 Hz) SIC rates, while it gets stronger in association with synaptic activity. In this latter case however, the possible increase in postsynaptic firing by astrocyte-mediated SICs, is limited by the rate of reintegration of released glutamate resources in the astrocyte (fixed at ∼1 Hz, Appendix B). Analogously to short-term synaptic depression in fact, our description of gliotransmitter release predicts that for release rates that exceed the rate of reintegration of released glutamate by the

astrocyte, exhaustion of astrocytic glutamate resources available for further release will result in SICs of smaller amplitude. In this fashion, due to depletion of astrocytic glutamate, the effect of large rates of glutamate release, and thus of SICs, on neuronal firing tends to be equivalent to that of considerably lower ones.

Taken together, the above results do not exclude a possible role of SICs in modulation of neuronal excitability and firing but suggest that such modulation could effectively occur only in coincidence with proper levels of synaptic activity. In this fashion, astrocyte-mediated SICs could be regarded to operate a sort of coincidence detection between synaptic activity and astrocytic glutamate release (Perea and Araque, 2005), whose readout would then be a temporally precise, cell-specific increase of neuronal firing (Figure 5F).

Astrocyte-mediated regulation of long-term plasticity

The strength of a synaptic connection between two neurons can be modified by activity, in a way that depends on the timing of neuronal firing on both sides of the synapse, through a series of processes collectively known as spike-timing–dependent plasticity (STDP) (Caporale and Dan, 2008). As both pre- and postsynaptic pathways of glutamatergic gliotransmission potentially change EPSC magnitude, thereby affecting postsynaptic firing, it may be expected that they could also influence STDP.

Although the molecular mechanisms of STDP remain debated, and different mechanisms could be possible depending on type of synapse, age, and induction protocol (Froemke et al., 2010), at several central excitatory synapses postsynaptic calcium concentration has been pointed out as a necessary factor in induction of synaptic changes by STDP (Magee and Johnston, 1997; Ismailov et al., 2004; Nevian and Sakmann, 2004; Bender et al., 2006; Nevian and Sakmann, 2006). Remarkably, amplitude and, likely, time course of postsynaptic Ca^{2+} could control the direction of plasticity: smaller, slower increases of postsynaptic Ca^{2+} give rise to spike-timing–dependent long-term depression (LTD) whereas larger, more rapid increases cause spike-timing–dependent long-term potentiation (LTP) (Magee and Johnston, 1997; Ismailov et al., 2004; Nevian and Sakmann, 2006). In calcium-based STDP models, this is also known as the "Ca^{2+}-control hypothesis" (Shouval et al., 2002; Cai et al., 2007; Graupner and Brunel, 2010). According to this hypothesis, no modification of synaptic strength occurs when Ca^{2+} is below a threshold θ_d that is larger than the resting Ca^{2+} concentration. If calcium resides in an intermediate concentration range, between θ_d and a second threshold $\theta_p > \theta_d$, the synaptic strength is decreased. Finally, if calcium increases above the second threshold, θ_p, the synaptic strength is potentiated.

Figures 6A.1 and 6B.1 exemplify the operational mechanism of the Ca^{2+}-control hypothesis within the framework of a nonlinear Ca^{2+}-based model for STDP at glutamatergic synapses originally introduced by Graupner and Brunel (2012). At most glutamatergic synapses, postsynaptic Ca^{2+} is mainly regulated by two processes: (i) postsynaptic Ca^{2+} entry mediated by NMDARs (Malenka and Bear, 2004), and (ii) Ca^{2+} influx by voltage-dependent Ca^{2+} channels (VDCCs) (Magee and Johnston, 2005; Bender et al., 2006; Nevian and Sakmann, 2006; Sjöström et al., 2008). In this fashion, each presynaptic action potential generates a long-lasting Ca^{2+} transient by opening NMDAR channels, while postsynaptic firing results in a short-lasting Ca^{2+} transient due to opening of VDCCs by dendritic depolarization through back-propagating action potentials (bAPs) (Caporale and Dan, 2008). Presynaptic action potentials alone do not trigger changes in synaptic strength, but they do so in correlation with postsynapitc bAPs (Sjöström and Nelson, 2002). Notably (Abbott and Nelson, 2000), in a typical STDP induction pairing protocol, LTD is induced if the postsynaptic neuron fires before the presynaptic one, i.e. post→pre pairing at negative spike timing intervals Δt (Figures 6A.1). Contrarily, LTP is

induced when the presynaptic cell fires before the postsynaptic cell, that is for pre→post pairing at positive Δt intervals (Figures 6A.1). This is possible because, when a presynaptic action potential is followed shortly after by a postsynaptic bAP, the strong depolarization by this latter drastically increases the voltage-dependent NMDAR-mediated Ca^{2+} current due to removal of the NMDAR magnesium block (Nowak et al., 1984; Jahr and Stevens, 1990), thereby resulting in supralinear superposition of the NMDAR- and VDCC-mediated Ca^{2+} influxes.

In the framework of the Ca^{2+}-control hypothesis, these observations may be summarized as follows. For large Δt, pre- and postsynaptic Ca^{2+} transients do not interact, and the contributions from potentiation and depression by pre/post pairs (or vice versa) cancel each other, leading to no synaptic changes on average (Figure 6C, *black curves*). For short, negative Δt, the presynaptically evoked Ca^{2+} transient rises instead above the depression threshold (θ_d) but not beyond the potentiation threshold (θ_p). Consequently, depression increases whereas potentiation remains constant, which leads to LTD induction. For short, positive Δt however, the postsynaptically evoked calcium transient rises on top of the presynaptic transient by the NMDAR nonlinearity, and increases activation of both depression and potentiation. Because the rate of potentiation is larger than the rate of depression (Appendix C), this results in LTP induction.

For the same number of pre/post pairs (or vice versa), mapping of the average synaptic modification as function of the spike timing interval Δt, ultimately provides an STDP curve that qualitatively resembles the classic curve originally described by Bi and Poo (1998) (Figure 6C, *bottom panel*, *black curve*). In the following, we will focus on parameters that lead to such a STDP curve and investigate how this curve is affected in the presence of glutamatergic gliotransmission, through the pre- and postsynaptic pathways of regulation discussed above.

Presynaptic pathway

The very nature of synaptic transmission crucially depends on the synapse's initial probability of neurotransmitter release insofar as this latter sets both the tone of synaptic transmission, that is how much neurotransmitter is released per action potential by the synapse on average, as well as whether the synapse displays short-term depression or facilitation (Abbott and Regehr, 2004). Synapses with low-to-intermediate values of initial neurotransmitter release probability, like for example, Schaffer collateral synapses (Dittman et al., 2000), or some cortical synapses (Markram et al., 1998b), are indeed prone to display facilitation, whereas synapses that are characterized by large release probability are generally depressing (Markram et al., 1998b). Because synaptic release probability also dictates the degree of activation of NMDARs, and consequently, the magnitude of postsynaptic Ca^{2+} influx, it is expected that both the tone of synaptic transmission and its short-term dynamics could affect STDP (Froemke et al., 2010). The relative weight of these two factors in shaping synaptic changes however, likely depends on the protocol for STDP induction. Short-term plasticity could indeed sensibly regulate STDP induction only for rates of presynaptic action potentials high enough to allow facilitation or depression of synaptic release from one AP to the following one (Froemke and Dan, 2002; Froemke et al., 2006). In this study, we consider low pre/post frequencies of 1 Hz. At such frequencies we expect short-term plasticity to have a negligible effect, and thus we only focus on how changes in the tone of synaptic transmission by glutamatergic gliotransmission affect STDP.

Figures 6A.2,B.2 respectively show the outcome of LTD and LTP induction for two consecutive pre→post and pre→post pairings preceded by the onset of release-decreasing gliotransmission at 0.1 s (*top panels*, *black marks*). A comparison of the ensuing postsynaptic Ca^{2+} dynamics with respect to the case without gliotransmission (Figures 6A.1,B.1) reveals that

the strong decrease of synaptic release probability (S.R.P., *top panels*, *red curves*) caused by gliotransmission remarkably reduces the NMDAR-mediated contribution to postsynaptic Ca^{2+} influx (*middle panels*), resulting in smaller variations of synaptic strength (*bottom panels*). In this fashion, at the end of the pairing protocol, release-decreasing gliotransmission accounts for less time spent by Ca^{2+} above either thresholds of LTD and LTP (Figure 6C, *top panel*, *red traces*). The resulting STDP curve thus displays strongly attenuated LTD and LTP (Figure 6C, *bottom panel*, *red curve*), with windows for these latter spanning a considerably smaller range of Δts than in the curve obtained without gliotransmission (*black curve*).

Similar considerations apply to the case of release-increasing gliotransmission (Figures 6A.3,B.3). In this case, the NMDAR component of postsynaptic Ca^{2+} could increase by gliotransmission even beyond the θ_d threshold (*dashed blue line*), thus favoring depression while reducing potentiation (*bottom panels*). In particular, for short positive Δt, the maximal LTP does not change but the Δt range for LTP induction shrinks. For $\Delta t > 40$ ms in fact, the time that Ca^{2+} spends above the LTD threshold increases with respect to the time spent by Ca^{2+} above the LTP threshold, thereby resulting in LTD induction (Figures 6C, *top panel*, *green traces*). In this fashion, the STDP curve in the presence of release-increasing gliotranmission displays a narrow 0–40 ms LTP window outside which LTD occurs instead (Figures 6C, *bottom panel*, *green curve*).

Figure 6D summarizes how the STDP curve changes for the whole spectrum of glutamatergic gliotransmission. In this figure, a y-axis value of "Gliotransmission Type" equal to 0 corresponds to maximum release-decreasing gliotransmission (*red curve* in Figure 3C); a value equal to 1 stands instead for maximum release-increasing gliotransmission (as in the case of the *green curve* in Figure 3C); finally, a value of 0.5 corresponds to no effect of gliotransmission on synaptic release (*black curve* in Figure 3C). It may be noted that gliotransmission may affect the STDP curve in several ways, changing both strength of plastic changes (*color code*) as well as shape and areas of LTP and LTD windows. In particular, as revealed by Figure 6E, maxima of LTP (*cyan circles*) and LTD (*yellow circles*) decrease with decreasing values of gliotransmission type, consistently with smaller postsynaptic Ca^{2+} influx for larger decreases of synaptic release by gliotransmission. This suggests that release-decreasing gliotransmission (*red-shaded area*) could attenuate STDP yet in a peculiar fashion, counteracting LTD more than LTP induction, as reflected by increasing values of LTP/LTD area ratio (*magenta curve*).

On the contrary, the effect of release-increasing gliotransmission (Figure 6E, *green-shaded area*) could be dramatically different. For sufficiently strong increases of synaptic release by gliotransmission in fact, the LTP/LTD area ratio drops to zero (*hatched area*) in correspondence with the appearance of two "open" LTD windows, one for $\Delta t < 0$ and the other for sufficiently large positive spike timing intervals. In parallel, consistently with the fact that release-increasing gliotransmission tends to increase the fraction of time spent by postsynaptic Ca^{2+} above the threshold for LTD thereby promoting this latter (Figure 6C), the range for LTP induction also tends to shrink to lower Δt values as release-increasing gliotransmission grows stronger (Figure 6D, *red color-coded areas* for Gliotransmission Type >0.5).

In summary, our analysis reveals that modulation of synaptic release by glutamatergic gliotransmission could change STDP both quantitatively and qualitatively, from hindering its induction for release-decreasing modulations, to altering both shape and existence of LTD windows for release-increasing modulations. However, whether and how this could effectively be observed in experiments remains to be investigated. Supported both by experimental evidence and theoretical arguments is the notion that regulations of the tone of synaptic transmission by glutamatergic gliotransmission likely require specific morphological and functional constraints to be fulfilled by the nature of astrocyte-synapse coupling (Araque et al., 2014; De Pittà et al., 2015). Similar arguments may ultimately hold true also for modulation of STDP, insofar as for this modulation

to be measured in our simulations, we required both a sufficiently strong increase/decrease of synaptic release by gliotransmission and a decay time of such increase/decrease long enough for this latter to be present during the induction protocol. Should these two aspects not have been fulfilled in our simulations, then modulations of STDP by gliotransmitter-mediated changes of synaptic release would likely have been negligible or even undetectable.

Postsynaptic pathway

We now turn our analysis to the possible impact of astrocyte-mediated SICs on STDP. Because SICs are through extrasynaptic NMDA receptors and these receptors are mainly permeable to Ca^{2+} ions (Cull-Candy et al., 2001), then SICs could contribute to postsynaptic Ca^{2+} thereby affecting STDP. Nevertheless, we should note that it is unclear whether and how extrasynaptic NMDARs contribute to plasticity, independently of the occurrence of SICs (Papouin and Oliet, 2014). For example, theta-burst LTP induction in CA1 neurons of rat hippocampal slices, is turned into LTD when extracellular NMDARs are selectively stimulated (Liu et al., 2013), but it is unknown whether these receptors have a role in STDP (Evans and Blackwell, 2015). In general, for a given STDP induction protocol, two factors that could crucially regulate how Ca^{2+} transients mediated by extrasynaptic NMDARs are involved in STDP, are the location of these receptors on the spine and the morphology of this latter in terms of spine head and neck (Bloodgood and Sabatini, 2007; Rusakov et al., 2004). Unfortunately both these factors remain unknown in the current knowledge of SIC-mediating extrasynaptic NMDARs and, for the remainder of this study, we assume that, in spite of their possible location away from the postsynaptic density along the spine neck or the dendritic shaft (Petralia et al., 2010), SIC-mediating extrasynaptic NMDARs could still regulate spine Ca^{2+} dynamics (Halassa et al., 2007a).

Based on the above rationale, we thus model SICs as slow potsynaptic Ca^{2+} transients that will add to presynaptically- and postsynaptically-triggered ones, and study their effect on the induction of SDTP by classic pairing protocols. For the sake of generality, we express the peak of SIC-mediated Ca^{2+} transients in units of NMDAR-mediated EPSCs. However, since in our STDP description individual EPSCs do not trigger any synaptic modification (Graupner and Brunel, 2012), then we may expect that only SICs sufficiently larger than EPSCs could effectively affect STDP. On the other hand, smaller SICs could also sum with Ca^{2+} transients by pre/post pairings resulting in Ca^{2+} elevations beyond either LTD or LTP thresholds that would ultimately cause synaptic changes (Figures 7A,B). Hence, based on these considerations, we deem amplitude and timing of SICs, both in terms of frequency of occurrence and onset with respect to STDP-inducing stimuli, to be crucial factors in shaping how SICs affect STDP, and thus we set to analyze these three factors separately.

Figure 7C summarizes the results of our simulations for SICs as large as 0.5, 1 or 1.5 times typical EPSCs, occurring at a fixed rate of 0.1 Hz and starting 100 ms before the delivery of 60 STDP-inducing pre/post pairings at 1 Hz. As illustrated in Figures 7A,B, for the same SIC kinetics, these simulations guarantee superposition between Ca^{2+} influxes mediated by SICs and pre/post pairings such that the extension of the ensuing Ca^{2+} transient beyond LTD and LTP thresholds (*dashed lines*) merely depends on SIC amplitude. In this fashion, it may be noted that SICs of amplitude smaller than or equal to typical EPSCs (Figure 7C, *turquoise circles* and *black circles* respectively), that alone would not produce any synaptic modification, do not sensibly change the STDP curve with respect to the previously considered case of an alike synapse in the absence of gliotransmission (Figure 6C, *black circles*). Conversely, large SICs could dramatically affect STDP, shifting the STDP curve towards negative synaptic changes (*blue circles*), and this negative shift increases the larger SICs grow beyond the θ_d threshold

(results not shown). In this case, STDP generally results in LTD with the exception of a LTP window that is comprised between ∼0 ms and positive Δt values that are smaller than those in the absence of gliotransmission (Figure 6C, *green circles*). This resembles what previously observed for STDP curves in the presence of release-increasing gliotransmission, with the only difference that, for large $|\Delta t|$ values, LTD strength in the presence of astrocyte-mediated SICs is found to be the same, regardless of Δt (compare the *blue curve* in Figure 7C with the *green curve* in Figure 6C).

In Figure 7D we consider the alternative scenario where only SICs as large as typical EPSCs impinge on the postsynaptic neuron at different rates, yet always 100 ms before STDP-inducing pairings. Akin to what happens for SIC amplitudes, the larger the SIC frequency is, the more the STDP curve changes. Indeed, as SIC frequency increases above SIC decay rate (i.e. $1/\tau_A$, Appendix A, Section A.1.4), SIC-mediated Ca^{2+} transients start adding up, so that the fraction of time spent by Ca^{2+} beyond the LTD threshold increases favoring LTD induction. In this fashion, the ensuing STDP curve, once again, consists of a narrow LTP window for $\Delta t \geq 0$, outside which only LTD is observed (*red curve*). In practice however, because SICs occur at rates that are much slower than their typical decay (Appendix B), they likely affect STDP in a more subtle fashion. This may be readily understood considering the *pink* STDP *curve* obtained for SICs at 0.1 Hz, that is the maximum rate experimentally recorded for these currents (Perea and Araque, 2005). Inspection of this curve indeed suggests that SICs could effectively modulate LTD and LTP maxima as well as the outer sides of the LTD/LTP windows, which dictate how fast depression/potentiation decay for large $|\Delta t|$, but overall the qualitative features of the STDP curve are preserved with respect to the case without gliotransmission (*black curve*).

Clearly, the extent of the impact of SIC amplitude and frequency on STDP discussed in Figures 7C,D ultimately depends on when SICs occur with respect to ongoing STDP-inducing pairings. Had we set SICs to occur ∼200 ms after pre/post Ca^{2+} transients in our simulations, then, as illustrated in Figures 7E,F, we would have not detected any sensible alteration of STDP, unless SICs were larger than typical EPSCs and/or occurred at sufficiently high rate to generate Ca^{2+} transients beyond the plasticity thresholds (results not shown). To seek understanding of how timing of SICs vs. pre/post pairings could alter LTD and/or LTP, we simulated STDP induction by pairing as the time interval ($\Delta\varsigma$) between SIC and pre/post pairs was systematically varied (with SIC rate fixed at 0.2 Hz) (Figures 7G–I). In doing so, we adopted the convention that negative $\Delta\varsigma$ values stand for SICs preceding pre/post (or post/pre) pairings while, positive $\Delta\varsigma$ refer to the opposite scenario of SICs that follow pairings (Figure 7G, *top schematics*). Then, it may be observed that, for $\Delta\varsigma$ in between approximately -300 ms and 0 ms, LTD could be induced for any negative Δt as well as for large positive Δt (Figure 7G, *blue tones*) – in this latter case to the detriment of the LTP window, whose upper bound moves to lower Δt values (Figure 7G, *red tones*). This results in STDP curves (e.g. Figure 7J, *yellow curve* for $\Delta\varsigma = -75$ ms) that bear strong analogy with the blue and red curves in Figures 7C,D respectively obtained for SICs of large amplitude and frequency, and suggest that depression grows as SICs tend to concur with pre/post pairings. An inspection of postsynaptic Ca^{2+} transients (Figures 7H,I) indeed reveals that coincidence of SICs and pre/post pairings, which occurs at negative $\Delta\varsigma$ of the order of SIC rise time (see Appendix B), corresponds to the longest time spent by Ca^{2+} above the LTD threshold, thereby resulting in maximum LTD (Figure 7K) and thus, minimum LTP (Figure 7L). Clearly, the $\Delta\varsigma$ range for which coincidence of SICs with pre/post pairings enhances LTD induction ultimately depends on kinetics of SICs, as reflected by their rise (τ_s^r) and/or decay time constants (τ_s), and spans $\Delta\varsigma$ values approximately comprised between ± SIC duration (i.e. $\simeq \tau_s^r + \tau_s$). As SIC duration increases in fact, either because of larger τ_s^r or larger τ_s or both, so does the $\Delta\varsigma$ range for LTD enhancement, as reflected by the *orange* and *blue curves* in Figures 7J–L.

In conclusion the simulations in Figures 7G–L point to both timing and duration of SICs with respect to pre/post pairing-mediated Ca^{2+} transients as a further, potentially-crucial factor in setting strength and polarity of STDP at glutamatergic synapses. It is noteworthy to emphasize that, however, to appreciate some effect on STDP, we had to assume in those simulations SICs occurring at 0.2 Hz, that is two-fold the maximum SIC rate (i.e. $\sim$ 0.1 Hz) experimentally observed (Perea and Araque, 2005). Indeed, analogous simulations run with realistic SIC rates $\leq$0.1 Hz did produce only marginal changes to STDP curves, akin to those previously observed for the pink STDP curve in Figure 7G. The potential functional implications (or lack thereof) of this perhaps puzzling result are addressed in the following Discussion.

Discussion

A large body of evidence has accumulated over the last years suggesting an active role of astrocytes in many brain functions. Collectively, these data fuelled the concept that synapses could be tripartite rather than bipartite, since in addition to the pre- and postsynaptic terminals, the astrocyte could be an active element in synaptic transmission (Araque et al., 1999; Haydon, 2001; Volterra and Meldolesi, 2005). Using a computational modeling approach, we showed here that glutamatergic gliotransmission could indeed play several roles in synaptic information transfer, either modulating synaptic filtering or controlling postsynaptic neuronal firing, as well as regulating both short- and long-term forms of synaptic plasticity. Supported by experimental observations (Liu et al., 2004b; Jourdain et al., 2007; D'Ascenzo et al., 2007; Bonansco et al., 2011; Perez-Alvarez et al., 2014), these results complement and extend previous theoretical work on astrocyte-mediated regulations of synaptic transmission and plasticity (De Pittà et al., 2013; De Pittà et al., 2015), and pinpoint biophysical conditions for a possible role of glutamatergic gliotransmission in spike-timing–dependent plasticity.

An important prediction of our model indeed is that both pathways of regulation of synaptic transmission by astrocytic glutamate considered in this study – presynaptic modulation of transmitter release and postsynaptic SICs – could affect STDP, potentially altering induction of LTP and LTD. This alteration could encompass changes in the timing between pre- and postsynaptic firing that is required for plasticity induction, as well as different variations of synaptic strength in response to the same stimulus. With this regard, the increase of LTP observed in our simulations, when moving from release-decreasing to release-increasing gliotransmission (Figure 6E), agrees with the experimental observation that LTP induction at hippocampal synapses requires weaker stimuli in the presence of endogenous glutamatergic gliotransmission rather than when gliotransmission is inhibited thereby decreasing synaptic release probability (Bonansco et al., 2011).

Notably, spike-timing–dependent plasticity in the hippocampus is not fully understood insofar as STDP induction by pairing protocols has produced a variety of seemingly contradicting observations for this brain region (Buchanan and Mellor, 2010). Recordings in hippocampal slices for example, showed that pairing of single pre- and postsynaptic action potentials at positive spike timing intervals could trigger LTP (Meredith et al., 2003; Buchanan and Mellor, 2007; Campanac and Debanne, 2008), as effectively expected by the classic STDP curve (Bi and Poo, 1998), but also induce either LTD (Wittenberg and Wang, 2006) or no plasticity at all (Buchanan and Mellor, 2007). Although different experimental and physiological factors could account for these diverse observations (Buchanan and Mellor, 2010; Shulz and Jacob, 2010), we may speculate that glutamatergic gliotransmission by astrocytes, which in those experiments was not explicitly taken into account, could also provide an alternative explanation. For example, the prediction of our model that release-increasing glutamatergic gliotransmission could account for multiple LTD windows, either at positive or negative spike timing intervals

(Figure 6), indeed supports the possibility that LTD in the hippocampus could also be induced by proper presentations of pre→post pairings sequences (Wittenberg and Wang, 2006). On the same line of reasoning, the possibility that astrocyte-mediated SICs could transiently increase postsynaptic firing (Figure 5F), could explain why, in some experiments, precise spike timing in the induction of synaptic plasticity in the hippocampus could exist only when single EPSPs are paired with postsynaptic bursts (Pike et al., 1999; Wittenberg and Wang, 2006). Moreover, it was also shown that postsynaptic firing is relatively less important than EPSP amplitude for the induction of STDP in the immature hippocampus compared to the mature network, possibly due to a reduced backpropagation of somatic APs in juvenile animals (Buchanan and Mellor, 2007). Remarkably, these diverse modes of plasticity induction could also ensue from different dynamics of glutamatergic gliotransmission, as likely mirrored by the developmental profile of somatic Ca^{2+} signals in hippocampal astrocytes (Volterra et al., 2014), which have been reported to be much more frequent in young mice (Sun et al., 2013). Insofar as somatic Ca^{2+} signals may result in robust astrocytic glutamate release that could trigger, in turn, similar increases of synaptic release and/or SICs (Araque et al., 2014; Sahlender et al., 2014), the frequent occurrence of these latter could then ultimately guarantee a level of dendritic depolarization sufficient to produce LTP in mice pups (Golding et al., 2002).

High amplitude/rate SICs, or large increases of synaptic release mediated by glutamatergic gliotransmission, result, in our simulations, in LTD induction for any spike timing interval except for a narrow LTP window at small-to-intermediate $\Delta t > 0$. This is in stark contrast with STDP experiments, where the observed plasticity always depends, to some extent, on the coincidence of pre- and postsynaptic activity, as EPSPs or postsynaptic action potentials fail to induce plasticity by their own (Sjöström and Nelson, 2002; Caporale and Dan, 2008). Apart from the consideration that large SIC amplitudes/rates and large increases of synaptic release by astrocytic glutamate may not reflect physiological conditions (Ding et al., 2007; Agulhon et al., 2008), this contrast may be further resolved on the basis of the following arguments.

A first consideration is that we simulated plasticity induction assuming either persistent occurrence of SICs or continuous modulations of synaptic release during the whole induction protocol. While this rationale proved useful to identify the possible mechanisms of regulation of STDP by glutamatergic gliotransmission, it may likely not reflect what occurs in reality. Indeed, modulations of synaptic release by glutamatergic gliotransmission could last only few tens of seconds (Fiacco and McCarthy, 2004; Jourdain et al., 2007) and thus be short-lived with respect to typical induction protocols which are of the order of minutes (Bi and Poo, 2001; Sjöström and Nelson, 2002; Sjöström et al., 2008). Moreover, the morphology of astrocytic perisynaptic processes is not fixed but likely undergoes dynamical reshaping in an activity-dependent fashion during plasticity induction (Lavialle et al., 2011; Perez-Alvarez et al., 2014), thereby potentially setting time and spatial range of action of gliotransmission on nearby synaptic terminals (De Pittà et al., 2015). In this fashion, LTD for large spike timing intervals could be induced only transiently and at selected synapses, focally targeted by glutamatergic gliotransmission, while leaving unchanged the qualitative features of the classic STDP curve obtained by somatic recordings in the postsynaptic neuron (Bi and Poo, 2001).

A further aspect that we did not take into account in our simulations is also the possible voltage dependence of astrocyte-triggered SICs. The exact nature of this dependence remains to be elucidated and likely changes with subunit composition of NMDA receptors that mediate SICs in different brain regions and at different developmental stages (Papouin and Oliet, 2014). Regardless, it may be generally assumed that slow inward currents through NMDA receptors become substantial only for intermediate postsynaptic depolarizations when the voltage-dependent Mg^{2+} block of these receptors is released (Jahr and Stevens, 1990). In this fashion, the possible effect of SICs on STDP would be confined in a time window around $\Delta t \geq 0$ for

which coincidence with pre- and postsynaptic spikes allows for robust depolarization of postsynaptic spines. Outside this window instead, SICs would be negligible, and plasticity induction would essentially depend on mere pre- and postsynaptic spiking rescuing the experimental observation of no synaptic modification for large spike timing intervals (Sjöström and Nelson, 2002; Caporale and Dan, 2008).

On the other hand, even without considering voltage-dependence of SIC-mediating NMDARs, the precise timing of SICs with respect to pre/post pairs, is predicted by our analysis, to be potentially critical in determining strength and sign of plasticity. And similar considerations could also hold for the onset time and duration of modulations of synaptic release triggered by gliotransmission with respect to the temporal features of plasticity-inducing stimuli (De Pittà et al., 2013). This ultimately points to timing of glutamate release by the astrocyte (and its downstream effects on synaptic transmission) as a potential additional factor for associative (Hebbian) learning, besides sole correlation between pre- and postsynaptic activities (Hebb, 1949; Gerstner and Kistler, 2002). Remarkably, this could also provide a framework to conciliate the possibility that modest, sporadic SICs that we predict would not substantially affect STDP (Figure 7), could do so instead (Chen et al., 2012). Indeed our predictions are based on the average number of SICs within a given time window as documented in literature rather than on the precise timing of those SICs in that time window. In this fashion for example, there is no distinction in terms of effect on STDP in our simulations, between a hypothetical scenario of three SICs randomly occurring on average every $\sim$10 s in a 30 s time frame and the alternative scenario of three SICs taking place within the same time frame but in rapid succession (Perea and Araque, 2005, Figure 5B), as could happen following an exocytic burst of glutamate release by the astrocyte (Marchaland et al., 2008; Santello et al., 2011; Sahlender et al., 2014). Yet the latter case could result in a dramatically different plasticity outcome with respect to the former. While individual SICs likely fail to induce synaptic modification alone in fact, their occurrence in rapid succession would instead allow postsynaptic Ca^{2+} levels to quickly increase beyond one of the thresholds for plasticity induction. Furthermore, this increase could further be boosted by coincidence of SICs with pre- and postsynpatic activity, ultimately accounting for robust LTP, as indeed predicted by other theoretical investigations (Wade et al., 2011). However, to complicate this intriguing scenario is the observation that glutamatergic gliotransmission (Santello et al., 2011), and even more so astrocyte-mediated SICs (Parri et al., 2001; Bardoni et al., 2010), are likely not deterministic but rather stochastic processes. Therefore, it would ultimately be interesting to understand how this stochasticity could affect neuronal activity and shape learning (Porto-Pazos et al., 2011).

To conclude, our analysis provides theoretical arguments in support of the hypothesis that, beyond neuronal firing, astrocytic gliotransmission could represent an additional factor in the regulation of activity-dependent plasticity and learning (Bains and Oliet, 2007; Min et al., 2012; De Pittà et al., 2015). This could occur in a variegated fashion by both presynaptic and postsynaptic elements targeted by glutamatergic gliotransmission, with possibly diverse functional consequences. Nonetheless, the practical observation in future experiments of a possible mechanism of action of glutamatergic gliotransmission on activity-dependent plasticity will depend on the implementation of novel specific plasticity-inducing protocols that match possible stringent temporal and spatial dynamical constraints defining the complex nature of neuron-astrocyte interactions.

Acknowledgements

M.D.P. wishes to thank Hugues Berry for insightful discussions, Marcel Stimberg, Romain Brette and members of Brette's group at the Institut de la Vision (Paris) for hospitality and

assistance in implementing simulations of this work in Brian 2.0. This work was supported by a FP7 Maria Skłodowska-Curie International Outgoing Fellowship to M.D.P. (Project 331486 "Neuron-Astro-Nets"). The authors declare no conflicts of interests.

Appendix A Modeling methods

A.1 Synapse model with glutamatergic gliotransmission

A.1.1 Synaptic release

To study modulation of short-term synaptic plasticity by gliotransmitter-bound extrasynaptically-located presynaptic receptors we extend the model originally introduced by De Pittà et al. (2011) for astrocyte-mediated heterosynaptic modulation of synaptic release to also account for the homosynaptic scenario. For the sake of clarity, in the following we will limit our description to excitatory (glutamatergic) synapses. Accordingly, synaptic glutamate release is described following Tsodyks (2005), whereby upon arrival of an action potential (AP) at time t_k, the probability of glutamate resources to be available for release (u_S) increases by a factor u_0, while the readily-releasable glutamate resources (x_S) decrease by a fraction $r_S(t_k) = u_S(t_k^+)x_S(t_k^-)$, corresponding to the fraction of effectively released glutamate. In between APs, glutamate resources are reintegrated at rate $1/\tau_d$ while u_S decays to zero at rate $1/\tau_f$. The equations for u_S, x_S thus read (Tsodyks, 2005)

$$\tau_f \frac{\mathrm{d}}{\mathrm{d}t} u_S = -u_S + \sum_k u_0(1-u_S)\,\delta(t-t_k)\tau_f \tag{1}$$

$$\tau_d \frac{\mathrm{d}}{\mathrm{d}t} x_S = 1 - x_S - \sum_k r_S(t)\,\delta(t-t_k)\tau_d \tag{2}$$

The parameter u_0 in the above equations may be interpreted as the synaptic release probability at rest. Indeed, when the period of incoming APs is much larger than the synaptic time scales τ_d, τ_f, in between APs $u_S \to 0$, $x_S \to 1$ – that is the synapse is "at rest" –, while, upon arrival of an AP, the probability of glutamate release from the synapse equals u_0.

A.1.2 Neurotransmitter time course

Assuming a total vesicular glutamate concentration of Y_T, the released glutamate, expressed as concentration in the synaptic cleft is then equal to $Y_{rel}(t_k) = \varrho_c\, Y_T\, r_S(t_k)$, where ϱ_c represents the ratio between vesicular and synaptic cleft volumes. The time course of synaptically-released glutamate in the cleft (Y_S) depends on several mechanisms, including clearance by diffusion, uptake and/or degradation (Clements, 1996; Diamond, 2005). In the simplest approximation, the contribution of these mechanisms to glutamate time course in the cleft may be modeled by a first order degradation reaction of characteristic time τ_c (Destexhe et al., 1994) so that

$$\tau_c \frac{\mathrm{d}}{\mathrm{d}t} Y_S = -Y_S + \sum_k Y_{rel}\,\delta(t-t_k)\tau_c \tag{3}$$

A.1.3 Astrocytic calcium dynamics

We assume that only a fraction ζ of released glutamate binds to postsynaptic receptors, while the remainder $1-\zeta$ fraction spills out of the cleft and activates astrocytic metabotropic receptors which trigger astrocytic Ca^{2+} signaling. The latter is modeled following Wallach et al. (2014) and results from the interplay of four quantities: (i) the fraction of activated astrocytic receptors

(γ_A); (ii) the cytosolic IP_3 (I) and (iii) Ca^{2+} concentrations (C) in the astrocyte; and (iv) the fraction of deinactivated IP_3 receptors (IP_3Rs) on the membrane of the astrocyte's endoplasmic reticulum (ER) that mediate Ca^{2+}-induced Ca^{2+}-released from this latter (h). In particular, considering each quantity separately, the fraction of astrocytic receptors bound by synaptic glutamate may be approximated, at first instance, by a first order binding reaction and thus evolves according to (Wallach et al., 2014)

$$\tau_A \frac{\mathrm{d}}{\mathrm{d}t}\gamma_A = -\gamma_A + O_M(1-\zeta)Y_S(1-\gamma_A)\tau_A \tag{4}$$

with τ_A representing the characteristic receptor deactivation (unbinding) time constant. Cytosolic IP_3 results instead from the complex Ca^{2+}-modulated interplay of phospholipase Cβ- and Cδ-mediated production and degradation by IP_3 3-kinase (3K) and inositol polyphosphatase 5-phosphatase (5P) (Zhang et al., 1993; Sims and Allbritton, 1998; Rebecchi and Pentyala, 2000; Berridge et al., 2003), and evolves according to the mass balance equation (De Pittà et al., 2009a)

$$\frac{\mathrm{d}}{\mathrm{d}t}I = J_\beta(\gamma_A) + J_\delta(C,I) - J_{3K}(C,I) - J_{5P}(I) \tag{5}$$

$$\tag{6}$$

where

$$J_\beta(\gamma_A) = O_\beta\,\gamma_A \qquad J_\delta(C,I) = O_\delta\,\frac{\kappa_\delta}{\kappa_\delta + I}\mathcal{H}\left(C^2, K_\delta\right)$$

$$J_{3K}(C) = O_{3K}\,\mathcal{H}\left(C^4, K_D\right)\mathcal{H}\left(I, K_3\right) \qquad J_{5P}(I) = \Omega_{5P}\,I$$

and $\mathcal{H}\left(x^n, K\right)$ denotes the sigmoid (Hill) function $x^n/(x^n + K^n)$. Finally, cytosolic Ca^{2+} and the IP_3R gating are described by a set of Hodgkin-Huxley-like equations according to the model originally introduced by Li and Rinzel (1994):

$$\frac{\mathrm{d}}{\mathrm{d}t}C = J_C(C,h,I) + J_L(C) - J_P(C) \tag{7}$$

$$\frac{\mathrm{d}}{\mathrm{d}t}h = \frac{h_\infty(C,I) - h}{\tau_h(C,I)} \tag{8}$$

where J_C, J_L, J_P respectively denote the IP_3R-mediated Ca^{2+}-induced Ca^{2+}-release from the ER (J_C), the Ca^{2+} leak from the ER (J_L), and the Ca^{2+} uptake from the cytosol back to the ER by serca-ER Ca^{2+}/ATPase pumps (J_P) (De Pittà et al., 2009a). These terms, together with the IP_3R deinactivation time constant (τ_h) and steady-state propability (h_∞), are given by (Li and Rinzel, 1994; De Pittà et al., 2009b)

$$J_C(C,h,I) = \Omega_C\,m_\infty^3 h^3\left(C_T - (1+\varrho_A)C\right) \qquad m_\infty(C,I) = \mathcal{H}\left(I, d_1\right)\mathcal{H}\left(C, d_5\right)$$

$$J_L(C) = \Omega_L\left(C_T - (1+\varrho_A)C\right) \qquad J_P(C) = O_P\mathcal{H}\left(C^2, K_P\right)$$

$$h_\infty(C,I) = d_2\frac{I+d_1}{d_2(I+d_1) + (I+d_3)C} \qquad \tau_h(C,I) = \frac{I+d_3}{\Omega_2(I+d_1) + O_2(I+d_3)C}$$

A detailed explanation of the parameters of the astrocyte model may be found in the Table in Appendix C.

A.1.4 Calcium-dependent glutamatergic gliotransmission

Astrocytic glutamate exocytosis is modeled akin to synaptic glutamate release, assuming that a fraction $x_A(t)$ of gliotransmitter resources is available for release at any time t. Then, every time t_j that astrocytic Ca^{2+} increases beyond a threshold concentration C_θ, a fraction of readily-releasable astrocytic glutamate resources, i.e. $r_A(t_j) = U_A\, x_A(t_j^-)$, is released into the periastrocytic space, and later reintegrated at rate $1/\tau_A$. Hence, $x_A(t)$ evolves according to (De Pittà et al., 2011)

$$\tau_G \frac{\mathrm{d}}{\mathrm{d}t} x_A = 1 - x_A - \sum_j r_A(t)\, \delta(t - t_j)\tau_G \tag{9}$$

Similarly to equation 3, we may estimate the contribution to glutamate concentration in the periastrocytic space (G_A), resulting from a quantal glutamate release event by the astrocyte at $t = t_j$, as $G_{rel}(t_j) = \varrho_e\, G_T\, r_A(t_j)$, where G_T represents the total vesicular glutamate concentration in the astrocyte, and ρ_e is the volume ratio between glutamate-containing astrocytic vesicles and periastrocytic space. Then, assuming a clearance rate of glutamate of $1/\tau_e$, the time course of astrocyte-derived glutamate in the extracellular space comprised between the astrocyte and the surrounding synaptic terminals is given by

$$\tau_e \frac{\mathrm{d}}{\mathrm{d}t} G_A = -G_A + \sum_j G_{rel}(t)\, \delta(t - t_j)\tau_e \tag{10}$$

A.1.5 Presynaptic pathway for glutamatergic gliotransmission

The extracellular glutamate concentration sets the fraction of bound extrasynaptically-located presynaptic receptors (γ_S) according to (De Pittà et al., 2011)

$$\tau_P \frac{\mathrm{d}}{\mathrm{d}t} \gamma_S = -\gamma_S + O_P\, (1 - \gamma_S) G_A \tau_P \tag{11}$$

where O_P and τ_P respectively denote the rise rate and the decay time of the effect of gliotransmission on synaptic glutamate release. It is then assumed that modulations of synaptic release by gliotransmitter-bound presynaptic receptors are brought forth by modulations of the resting synaptic release probability, i.e. $u_0 = u_0(\gamma_S)$. In an attempt to consider a mechanism as general as possible, rather than focusing on a specific functional dependence for $u_0(\gamma_S)$, we consider only the first order expansion of this latter (De Pittà et al., 2011), that is

$$u_0(\gamma_S) \approx U_0 + (\xi - U_0)\gamma_S \tag{12}$$

where U_0 denotes the synaptic release probability at rest in the absence of gliotransmission, whereas the parameter ξ lumps, in a phenomenological way, the information on the effect of gliotransmission on synaptic release. For $0 \leq \xi < U_0$, u_0 decreases with γ_S, consistent with a "release-decreasing" effect of astrocytic glutamate on synaptic release. This could be the case, for example, of astrocytic glutamate binding to presynaptic kinate receptors or group II/III mGluRs (Araque et al., 1998a; Liu et al., 2004b,a). Vice versa, for $U_0 < \xi \leq 1$, u_0 increases with γ_S, consistent with a "release-increasing" effect of astrocytic gliotransmitter on synaptic release, as in the case of presynaptic NMDARs or group I mGluRs (Fiacco and McCarthy, 2004; Jourdain et al., 2007; Perea and Araque, 2007; Navarrete and Araque, 2010; Bonansco et al., 2011; Navarrete et al., 2012a; Perea et al., 2014). Finally, the special case where $\xi = U_0$ corresponds to occlusion, that is coexistence and balance between release-decreasing and release-increasing glutamatergic gliotransmission at the same synapse resulting in no net effect of this

latter on synaptic release.

Although based on glutamatergic synapses, the set of equations 1–12 provides a general description for modulations of synaptic release mediated by glutamatergic gliotransmission that could also be easily extended to other types of excitatory synapses (Pankratov et al., 2007) as well as inhibitory synapses (Kang et al., 1998; Serrano et al., 2006; Liu et al., 2004a; Losi et al., 2014).

A.1.6 Postsynaptic pathways for glutamatergic gliotransmission: slow inward currents

Postsynaptic astrocyte-mediated slow inward currents take place through extrasynaptic NMDA receptors. The subunit composition of these receptors however remains unclear (Papouin and Oliet, 2014). Several studies reported SICs to be inhibited by antagonists of NR2B-containing NMDARs (Fellin et al., 2004; Shigetomi et al., 2008; Pirttimaki et al., 2011), there is also evidence that other NMDAR types could be involved possibly subunits could be involved such as NR2C or NR2D (Bardoni et al., 2010). Being mediated by NMDA receptors, SICs are likely affected by voltage-dependence of the Mg^{2+} block of these receptors. Although there is evidence that SICs rate and frequency could indeed depend on extracellular Mg^{2+} (Fellin et al., 2004), the effective nature of the possible voltage dependence of SICs has not been elucidated. Moreover, the potential diversity of subunit composition of receptors mediated SICs could also result in different voltage dependencies, strong for NR2B-containing receptors, akin to postsynaptic NMDARs, and weak otherwise (Cull-Candy et al., 2001). Accordingly, in this study we neglect the possible voltage-dependence of SICs arguing that this is not substantially changing the essence of our results (see Discussion). In this fashion, denoting postsynaptic SICs by $i_A(t)$, we model them by a difference of exponentials according to

$$\tau_S^r \frac{\mathrm{d}}{\mathrm{d}t} i_A(t) = -i_A(t) + \hat{I}_A B_A(t)\, \tau_S^r \tag{13}$$

$$\tau_S \frac{\mathrm{d}}{\mathrm{d}t} B_A(t) = -B_A(t) + \hat{J}_A G_A(t)\, \tau_S \tag{14}$$

where τ_S^r, τ_S respectively are rise and decay time constants for SICs. The two scaling factors $\hat{I}_A$, $\hat{J}_A$ are taken such that the SIC maximum in correspondence with an event of glutamate release by the astrocyte is equal to a constant value I_A (see Appendix B).

A.1.7 Postsynaptic neuron

Postsynaptic action potential firing is modeled by a leaky integrate-and-fire (LIF) neuron (Burkitt, 2006; Fourcaud and Brunel, 2002). Accordingly, the membrane potential (v) of the postsynaptic neuron evolves as

$$\tau_m \frac{\mathrm{d}}{\mathrm{d}t} v = E_L - v + i_S(t) + i_A(t) \tag{15}$$

where τ_m denotes the membrane time constant and $i_S(t)$ represents the excitatory synaptic input to the neuron. Every time v crosses the firing threshold v_θ, an AP is emitted and the membrane potential is reset to v_r and kept at this value for the duration of a refractory period τ_r.

For synaptic currents, we only consider the AMPA receptor-mediated fast component of EPSCs. Accordingly, we consider two possible descriptions for $i_S(t)$. In Figures 3 and 4, we assume that the rise time of synaptic currents is very short compared to the relaxation time of these latter (Spruston et al., 1995; Magee and Cook, 2000; Andrásfalvy and Magee, 2001), so

that $i_S(t)$ can be modeled by a sum of instantaneous jumps of amplitude $\hat{J}_S$, each followed by an exponential decay (Fourcaud and Brunel, 2002), i.e.

$$\tau_N \frac{\mathrm{d}}{\mathrm{d}t} i_S(t) = -i_S(t) + \hat{J}_S \zeta Y_S(t)\, \tau_N \tag{16}$$

In the presence of gliotransmitter-mediated slow-inward currents instead (Figure 5), we model synaptic currents similarly to these latter, that is

$$\tau_N^r \frac{\mathrm{d}}{\mathrm{d}t} i_S(t) = -i_S(t) + \hat{I}_S B_S(t)\, \tau_N^r \tag{17}$$

$$\tau_N \frac{\mathrm{d}}{\mathrm{d}t} B_S(t) = -B_S(t) + \hat{J}_S \zeta Y_S(t)\, \tau_N \tag{18}$$

where τ_N^r, τ_N respectively denote EPSC rise and decay time constants; the scaling factor $\hat{J}_S$ is taken such that synaptic releases result in unitary increases of the gating variable B_S, and similarly, $\hat{I}_S$ is set such that an increases in synaptic current ensuing from quantal synaptic release equals to I_S.

A.2 Spike-timing–dependent plasticity

A.2.1 Postsynaptic calcium dynamics

Spike-timing–dependent plasticity is modeled by the nonlinear calcium model introduced by Graupner and Brunel (2012), which was modified to include short-term synaptic plasticity as well as astrocyte-mediated SIC contribution to postsynaptic Ca^{2+}. Accordingly, postsynaptic Ca^{2+} dynamics, $c(t)$, results from the sum of three contributions: (i) Ca^{2+} transients mediated by NMDA receptors, activated by synaptic glutamate whose release probability from the presynaptic bouton may be modulated by gliotransmission (c_{pre}), (ii) Ca^{2+} transients mediated by gliotransmitter-triggered NMDA-mediated SICs (c_{sic}), (iii) Ca^{2+} transients due to activation of voltage-dependent Ca^{2+} channels (VDCCs) by postsynaptic backpropagating APs (c_{post}). All three Ca^{2+} transients are accounted for by a difference of exponentials. In particular, presynaptic Ca^{2+} transients are described by

$$\tau_{pre}^r \frac{\mathrm{d}}{\mathrm{d}t} c_{pre} = -c_{pre} + \hat{C}_{pre} R_{pre} \tau_{pre}^r \tag{19}$$

$$\tau_{pre} \frac{\mathrm{d}}{\mathrm{d}t} R_{pre} = -R_{pre} + W_N\, \zeta\, Y_S\, \tau_{pre} \tag{20}$$

where τ_{pre}^r, τ_{pre} are rise and decay time constants of the Ca^{2+} transient; $\hat{C}_{pre}$ is a normalization constant such that the maximal amplitude of the transient is C_{pre}; W_N is the "weight" of presynaptic Ca^{2+} transients triggered by synaptic glutamate (Y_S, equation 3).

Similarly to presynaptic ones, calcium transients due to by SICs mediated by gliotransmission are given by

$$\tau_{sic}^r \frac{\mathrm{d}}{\mathrm{d}t} c_{sic} = -c_{sic} + \hat{C}_{sic} R_{sic} \tau_{sic}^r \tag{21}$$

$$\tau_{sic} \frac{\mathrm{d}}{\mathrm{d}t} R_{sic} = -R_{sic} + W_A\, G_A\, \tau_{sic} \tag{22}$$

where τ_{sic}^r, τ_{sic}^d are the rise and decay time constants of the Ca^{2+} transient; and $\hat{C}_{sic}$ is a normalization constant such that the maximal amplitude of the transient is C_{sic}; W_A is the "weight" of SIC-mediated Ca^{2+} transients triggered by perisynaptic gliotransmitter (G_A, equation 10).

Finally, postsynaptic Ca^{2+} transients caused by bAPs are modeled by (Graupner and Brunel, 2012)

$$\tau^r_{post}\frac{\mathrm{d}}{\mathrm{d}t}c_{post} = -c_{post} + \hat{C}_{post}R_{post}\tau^r_{post} \tag{23}$$

$$\tau_{post}\frac{\mathrm{d}}{\mathrm{d}t}R_{post} = -R_{post} + (1+\eta c_{pre})\sum_i \delta(t-t_i)\tau_{post} \tag{24}$$

where the sum goes over all postsynaptic APs occurring at times t_i; τ^r_{post}, τ_{post} are the rise and decay time constants of the Ca^{2+} transient; $\hat{C}_{post}$ is a scaling factor such that the maximal amplitude of the transient is C_{post}, and the parameter η implements by which amount the bAP-evoked Ca^{2+} transient is increased in case of preceding presynaptic stimulation.

A.2.2 Synaptic efficacy

The temporal evolution of synaptic efficacy $\rho(t)$ depends on postsynaptic Ca^{2+} dynamics $c(t) = c_{pre}(t) + c_{sic}(t) + c_{post}(t)$ and is described by the first-order differential equation (Graupner and Brunel, 2012)

$$\tau_\rho\frac{\mathrm{d}}{\mathrm{d}t}\rho = -\rho(1-\rho)(\rho_\star-\rho) + \gamma_p(1-\rho)\Theta\left(c(t)-\theta_p\right) - \gamma_d\,\rho\,\Theta\left(c(t)-\theta_d\right) + \mathrm{Noise}(t) \tag{25}$$

where $\rho_\star$ is the boundary of the basins of attraction of UP and DOWN states of synaptic efficacy, that is the states for which $\rho = 1$ and $\rho = 0$ respectively; θ_d, θ_p denote the depression (LTD) and potentiation (LTP) thresholds, and γ_d, γ_p measure the corresponding rates of synaptic decrease and increase when these thresholds are exceeded; $\Theta(\cdot)$ denotes the Heaviside function, i.e. $\Theta\left(c-\theta\right) = 0$ for $c < \theta$ and $\Theta\left(c-\theta\right) = 1$ for $c \geq \theta$. The last term lumps an activity-dependent noise term in the form of $\mathrm{Noise}(t) = \sigma\sqrt{\tau_\varrho}\sqrt{\Theta\left(c(t)-\theta_d\right)+\Theta\left(c(t)-\theta_p\right)}\cdot\varpi(t)$ where $\varpi(t)$ is a Gaussian white noise process with unit variance density. This term accounts for activity-dependent fluctuations stemming from stochastic neurotransmitter release, stochastic channel opening and diffusion (Graupner and Brunel, 2012).

A.3 STDP curves

To construct the STDP curves of Figures 6 and 7, we follow the rationale originally described by Graupner and Brunel (2012), and consider the average synaptic strength of a synaptic population after a stimulation protocol of n pre-post (or post-pre) pairs presented at time interval T. With this aim, synaptic strength is surmised to be linearly related to ρ as $w = w_0 + \rho(w_1 - w_0)$, where w_0, w_1 are the synaptic strength of the DOWN/UP states for which ρ_0, i.e. the initial value of ρ at $t = 0$, is 0 or 1 respectively. In this fashion, w may be thought as a rescaled version of equivalent experimental measures of synaptic strength such as the excitatory postsynaptic potential (EPSP) or current (EPSC) amplitude, the initial EPSP slope or the current in a 2-ms windows at the EPSC peak. Accordingly, before a stimulus protocol, a fraction β of the synapses is taken in the DOWN state, so that the average initial synaptic strength is $\bar{w}_0 = \beta\, w_0 + (1-\beta)w_1$. Then, after the stimulation protocol, the ensuing average synaptic strength is $\bar{w}_1 = w_0((1-\mathcal{U})\beta + \mathcal{D}(1-\beta)) + w_1(\mathcal{U}\beta + (1-\mathcal{D})(1-\beta))$ where $\mathcal{U}$, $\mathcal{D}$ represent the UP and DOWN transition probabilities respectively. As in experiments, we consider the change in synaptic strength as the ratio between the average synaptic strengths after and before the stimulation, i.e.

$$\Delta\varrho = \frac{(1-\mathcal{U})\beta + \mathcal{D}(1-\beta) + b(\mathcal{U}\beta + (1-\mathcal{D})(1-\beta))}{\beta + (1-\beta)b} \tag{26}$$

with $b = w_1/w_0$. Under the hypotheses of this study, that $T \ll \tau_\varrho$ and γ_d, γ_p are large, the transition probabilities $\mathcal{U}$, $\mathcal{D}$ may be analytically solved and read (Graupner and Brunel, 2012)

$$\mathcal{U}(\rho_0) = \frac{1}{2}\left(1 + \mathrm{erf}\left(-\frac{\rho_\star - \bar{\rho} + (\rho - \rho_0)\mathrm{e}^{-\frac{nT}{\tau}}}{\sqrt{\sigma_\rho}\left(1 - \mathrm{e}^{-\frac{2nT}{\tau}}\right)}\right)\right) \tag{27}$$

$$\mathcal{D}(\rho_0) = \frac{1}{2}\left(1 - \mathrm{erf}\left(-\frac{\rho_\star - \bar{\rho} + (\rho - \rho_0)\mathrm{e}^{-\frac{nT}{\tau}}}{\sqrt{\sigma_\rho}\left(1 - \mathrm{e}^{-\frac{2nT}{\tau}}\right)}\right)\right) \tag{28}$$

where erf denotes the standard Error Function, defined as $\mathrm{erf}(x) = \frac{2}{\sqrt{\pi}}\int_0^x \mathrm{e}^{-t^2}\mathrm{d}t$ and

$$\bar{\rho} = \frac{\Gamma_p}{\Gamma_d + \Gamma_p}, \qquad \sigma_\rho^2 = \frac{\alpha_d + \alpha_p}{\Gamma_d + \Gamma_p}\sigma^2, \qquad \tau = \frac{\tau_\rho}{\Gamma_d + \Gamma_p}$$

with $\Gamma_i = \gamma_i\,\alpha_i$ and $\alpha_i = \frac{1}{nT}\int_0^{nT}\Theta\left(c(t) - \theta_i\right)\mathrm{d}t$ with $i = d,\, p$.

A.4 Simulations

The model was implemented in Brian 2.0 (Stimberg et al., 2014). Simulations and data analysis were serendipitously designed and performed by the open source programming language Python 2.7 (Python Software Foundation, 2015). The code is available online at <*add url*>.

Appendix B Parameter estimation

B.1 Synaptic parameters

Glutamate release probability U_0 of central excitatory synapses is generally comprised between ∼0.09 (Schikorski and Stevens, 1997) and ∼0.6–0.9 (Stevens and Wang, 1995; Markram et al., 1998a), with lower values mostly consistent with facilitating synapses (Murthy et al., 1997). Facilitation time constants τ_f may be estimated by the decay time of intracellular Ca^{2+} increases at presynaptic terminals upon arrival of action potentials (Regehr et al., 1994; Emptage et al., 2001). With this regard, typical decay times for Ca^{2+} transients are reported to be <500 ms (Emptage et al., 2001), with an upper bound between 0.65–2 s (Regehr et al., 1994). Concerning depression time constants instead, experiments have reported glutamate-containing vesicles in the readily releasable pool to preferentially undergo rapid endocytosis within 1–2 s after release (Pyle et al., 2000), although vesicle recycling could also be as fast as 10–20 ms (Stevens and Wang, 1995; Brody and Yue, 2000).

Estimates in hippocampal synapses suggest that the readily releasable pool could count between 2 and 27 vesicles (Schikorski and Stevens, 1997) which are essentially spherical with average outer diameter d_S equal to 39.2±11.4 nm and in the range of 23–49 nm (Harris and Sultan, 1995; Bergersen et al., 2012). Subtracting to this value a 6 nm-thick vesicular membrane (Schikorski and Stevens, 1997), the inner diameter of a vesicle can then be estimated between 16–38 nm, corresponding to a mean vesicular volume Λ_S in the range of $2.1 \cdot 10^{-21}$–$28.7 \cdot 10^{-21}$ dm^3. Given that vesicular glutamate concentration is reported in the range of 60–210 mM (Harris and Sultan, 1995; Danbolt, 2001; Bergersen et al., 2012), then considering a pool of 10 vesicles with average diameter of 30 nm (i.e. average volume $\Lambda_S \approx 14.1 \cdot 10^{-21}$ dm^3) and average vesicular neurotransmitter concentration of 60–100 mM (Bergersen et al., 2012), the total neurotransmitter vesicular content ranges up to $Y_T = (10)(60\text{–}100 \text{ mM}) = 300\text{–}1000$ mM. Assuming a typical neurotransmitter release time of $t_{rel} = 25$ μs (Raghavachari and Lisman, 2004) and a diffusion constant for glutamate in the synaptic cleft of $D_{\text{Glu}} = 0.33$ $\mu m^2/ms$ (Nielsen et al., 2004), the average diffusion length (ℓ_c) of a glutamate molecule from the release site can be estimated by the Einstein-Smoluchowski relationship (Schikorski and Stevens, 1997) whereby $\ell_c = \sqrt{(2 \cdot D_{\text{Glu}} \cdot t_{rel})} = \sqrt{(2 \cdot 0.33\ \mu m^2/ms \cdot 0.025\ ms)} \approx 0.129$ μm. Thus, the associated mixing volume Λ_c, namely the effective diffusion volume which the released glutamate has rapid access to, can be estimated by the volume of the disk of radius ℓ_c and thickness h_c equal to the average width of the synaptic cleft (Barbour, 2001). Considering $h_c = 20$ nm (Schikorski and Stevens, 1997), it is: $\Lambda_c = \pi\, \ell_c^2 h_c = \pi \cdot (0.129\ \mu m)^2 (0.020\ \mu m) \approx 8.89 \cdot 10^{-18}$ dm^3 which falls in the experimental range of volumes of nonsynaptic interfaces at hippocampal synapses elsewhere reported (Ventura and Harris, 1999). Considering vesicular release from at least 3 independent sites (Oertner et al., 2002), it follows that the ratio between vesicle volume and mixing volume is $\varrho_c = \Lambda_S/\Lambda_c = (3)(14.1 \cdot 10^{-21}\ dm^3)/(8.89 \cdot 10^{-18}\ dm^3) \approx 0.005$, so that the contribution to the concentration of glutamate in the extracellular space following a release event, is $Y_{rel} = \rho_c \cdot U_0 \cdot Y_T$. Hence, for a sample value of $U_0 = 0.5$ (Stevens and Wang, 1995) with a choice of $Y_T = 500$ mM for example, the latter equals to $Y_{rel} = (0.005)(0.5)(500 \text{ mM}) \approx 1.25$ mM.

Such released glutamate is then rapidly cleared from the extracellular space by combined action of diffusion and uptake by transporters (Barbour and Häusser, 1997). As a result the time course of glutamate in the synaptic cleft is short, with an estimated decay constant between ∼2–10 ms (Clements et al., 1992; Diamond, 2005). However, slower clearance times could also be possible since resting glutamate concentrations in the extracellular space surrounding activated synapses are recovered only ∼100 ms after the stimulus (Herman and Jahr, 2007; Okubo et al., 2010). Based on these considerations, we consider an intermediate value of glutamate clearance time of $\tau_c = 25$ ms.

B.2 Astrocyte parameters

Astrocyte parameters reported in Appendix C were estimated on extensive numerical explorations of the astrocyte model aimed at reproducing experimental whole-cell Ca^{2+} elevations with rise and decay time constants respectively in the ranges of 3–20 s and 3–25 s and with full-width half-maximum (FWHM) values between 5–160 s (Hirase et al., 2004; Nimmerjahn et al., 2004; Wang et al., 2006). In doing so, we considered a ratio between ER and cytoplasmic volumes (ϱ_A) of 0.18 in line with the experimental observation that the probability of ER localization in the cytoplasmic space at astrocytic somata is between ∼20–70% (Pivneva et al., 2008). Moreover, the cell's total Ca^{2+} concentration (measured with respect to the cytoplasmic volume) was fixed at $C_T = 2$ μM, while Ca^{2+} affinity of sarco-ER pumps (SERCAs) was taken equal to 0.05 μM (Lytton et al., 1992; Vandecaetsbeek et al., 2009), assuring peak Ca^{2+} concentrations <5 μM in agreement with experiments (Parpura and Haydon, 2000; Kang and Othmer, 2009).

Activation rate and unbinding time constants O_A, τ_A of astrocytic receptors may be estimated by rise times of agonist-triggered Ca^{2+} signals. With this regard, application of 50 μM of DHPG, a potent agonist of group I subtype 5 mGluRs – the main type of mGluRs expressed by astrocytes (Aronica et al., 2003) –, triggered submembrane Ca^{2+} signals characterized by a rise time $\tau_r = 0.272 \pm 0.095$ s. Because mGluR5 affinity ($K_{0.5}$) for DHPG is ∼2 μM (Brabet et al., 1995), that is much smaller than the applied agonist concentration, receptor saturation may be assumed in those experiments so that the receptor activation rate by DHPG (O_{DHPG}) can be expressed as a function of τ_r (Barbour, 2001) whereby $O_{\mathrm{DHPG}} \approx \tau_r(50\ \mu\mathrm{M})^{-1} = 0.055$–$0.113\ \mu\mathrm{M}^{-1}\mathrm{s}^{-1}$ and, accordingly, $\Omega_{\mathrm{DHPG}} = 1/O_{\mathrm{DHPG}}K_{0.5} \approx$ 4–10 s. Corresponding rate constants for glutamate may then be estimated by the latter, assuming similar kinetics yet with $K_{0.5} = K_A = 1/O_A\tau_A \approx$ 3–10 μM (Daggett et al., 1995), that is 1.5–5-fold larger than $K_{0.5}$ for DHPG. Moreover, since rise times of Ca^{2+} signals triggered by non-saturating physiological stimuli are somehow faster than in the case of DHPG (Panatier et al., 2011), it may be assumed that $O_N > O_{\mathrm{DHPG}}$. With this regard, for a choice of $O_A \approx 3\,O_{\mathrm{DHPG}} = 0.3\ \mu\mathrm{M}^{-1}\mathrm{s}^{-1}$, with $K_A = 6$ μM such that $\tau_A = 1/(0.3\ \mu\mathrm{M}^{-1}\mathrm{s}^{-1})/(6\ \mu\mathrm{M}) = 0.55$ s, a peak synaptic glutamate concentration of $Y_{rel} = 1200$ μM, with $\tau_c = 25$ ms results in a maximum average fraction of bound receptors of ∼0.75–0.9 that occurs within ≈ 70 ms from synaptic release, in good agreement with experimentally-reported rise times.

B.3 Gliotransmission

Exocytosis of glutamate from astrocytes is reported to occur by Ca^{2+} concentrations increasing beyond a threshold value $C_\theta \approx 0.15-0.8$ μM. In this study we specifically consider $C_\theta = 0.5$ μM. Glutamate-containing vesicles found in astrocytic processes have regular (spherical) shape with typical diameters (d_A) between ∼20–110 nm (Bezzi et al., 2004; Crippa et al., 2006). The corresponding vesicular volume Λ_A then is between ∼2–700·10^{-21} dm^3. Vesicular glutamate content is approximately the same, or at least as low as one third of synaptic vesicles in adjacent nerve terminals (Montana et al., 2006; Jourdain et al., 2007; Bergersen et al., 2012). Thus, considering a range of synaptic vesicular glutamate content between ∼60–150 mM (Danbolt, 2001), astrocytic vesicular glutamate concentration (G_v) is likely within ∼20–150 mM (Bergersen et al., 2012).

The majority of glutamate vesicles in astrocytic processes clusters in close proximity to the plasma membrane, i.e. <100 nm, but about half of them is found within a distance of 40–60 nm from the ventral side of the membrane, suggesting existence of "docked" vesicles in astrocytic processes akin to synaptic terminals (Jourdain et al., 2007; Bergersen et al., 2012). Borrowing the synaptic rationale whereby docked vesicles approximately correspond to readily releasable

ones (Schikorski and Stevens, 1997), then the average number of astrocytic glutamate vesicles available for release (n_A) could be between ∼1–6 (Jourdain et al., 2007). Hence, the total vesicular glutamate releasable by an astrocyte may be estimated between $G_T = n_A G_A = 20$–900 mM.

Astrocytic vesicle recycling (τ_G) likely depends on the mode of exocytosis. Both full-fusion of vesicles and kiss-and-run events have been observed in astrocytic processes (Bezzi et al., 2004) with the latter seemingly occurring more often (Bezzi et al., 2004; Chen et al., 2005). The fastest recycling pathway corresponds to kiss-and-run fusion, where the rate is mainly limited by vesicle fusion with plasma membrane and subsequent pore opening (Valtorta et al., 2001). Indeed, reported pore-opening times in this case, can be as short as 2.0±0.3 ms (Chen et al., 2005). The actual recycling time however, could be considerably longer if we take into account that, even for fast release events confined within 100 nm from the astrocyte plasma membrane, vesicle re-acidification could last ∼1.5 s (Bowser and Khakh, 2007).

Considering a value for the diffusion constant of glutamate in the extracellular space of $D_{\mathrm{Glu}} = 0.2\ \mu\mathrm{m}^2/\mathrm{ms}$ (Nielsen et al., 2004), and a vesicle release time $t_{rel} \approx 1$ ms (Chen et al., 2005), the average diffusion distance travelled by astrocytic glutamate molecules into the extracellular space is (Schikorski and Stevens, 1997) $\ell_e = \sqrt{(2 \cdot 0.2\ \mu\mathrm{m}^2/\mathrm{ms} \cdot 1\ \mathrm{ms})} \approx 0.63\ \mu\mathrm{m}$. Then, assuming that the mixing volume of released glutamate Λ_e in the extracellular space coincides with one tenth (i.e. 0.1) of the ideal diffusion volume in free space (Rusakov and Kullmann, 1998), it is $\Lambda_e = (0.1)\, 4\,\pi\, \ell_e^3/3 \approx 10^{-16}\ \mathrm{dm}^3$. Accordingly, considering an average vesicular diameter $d_A = 50$ nm, so that $\Lambda_A \approx 65 \cdot 10^{-21}\ \mathrm{dm}^3$, the ratio ϱ_e between vesicular and mixing volumes for astrocytic glutamate diffusion can be estimated to be of the order of $\varrho_e = \Lambda_A/\Lambda_e = (65 \cdot 10^{-21}\ \mathrm{dm}^3)/10^{-16}\ \mathrm{dm}^3 \approx 6.5 \cdot 10^{-4}$. For an astrocytic pool of releasable glutamate of $G_T = 200$ mM, and a release probability $U_A = 0.6$, it follows that the extracellular peak glutamate concentration after exocytosis is $\hat{G}_A = (6.5 \cdot 10^{-4})(0.6)(200\ \mathrm{mM}) \approx 78\ \mu\mathrm{M}$, in agreement with experimental measurements (Innocenti et al., 2000). Finally, imaging of extrasynaptic glutamate dynamics in hippocampal slices hints that glutamate clearance is fast and mainly carried out within <300 ms of exocytosis (Okubo et al., 2010). Therefore, we consider a characteristic clearance time constant for glutamate in the periastrocytic space of $\tau_e = 200$ ms.

B.4 Presynaptic receptors

We set the activation rate and inactivation time constants of presynaptic-receptors, i.e. O_P and τ_P, to reproduce the experimentally-reported rapid onset of the modulatory effect on synaptic release exerted by those receptors, namely within 1–5 s from glutamate exocytosis by the astrocyte, and the slow decay of this modulation, which is of the order of tens of seconds at least (Fiacco and McCarthy, 2004; Jourdain et al., 2007). In particular, inhibition of synaptic release following activation of presynaptic mGluRs by astrocytic glutamate could last from tens of seconds (Araque et al., 1998a) to ∼2–3 min (Liu et al., 2004b). Similarly, group I mGluR–mediated enhancement of synaptic release following a single Ca^{2+} elevation in an astrocyte process, may last as long as ∼30–60 s (Fiacco and McCarthy, 2004; Perea and Araque, 2007). Values within ∼1–2 min however, have also been reported in the case of an involvement of NMDARs (Araque et al., 1998b; Jourdain et al., 2007). No specific assumption is made on the possible ensuing peak of receptor activation by a single glutamate release by the astrocyte.

B.5 Postsynaptic neuron

The membrane time constant of pyramidal neurons is typically between 20–70 ms (Pankratov and Krishtal, 2003; Routh et al., 2009) in correspondence of a membrane potential at rest in the range of −66.5±11.7 mV (Spruston et al., 1995; Magee, 1998; Magee and Cook, 2000; Otmakhova et al., 2002; Gasparini et al., 2004; McDermott et al., 2006; Routh et al., 2009).

Firing threshold (v_θ) values are on average around -53 ± 2 mV (McDermott et al., 2003; Gasparini et al., 2004; Gasparini and Magee, 2006), ensuing in after-spike reset potentials (v_r) of $2-3$ mV smaller (Gasparini et al., 2004; Metz et al., 2005; Routh et al., 2009). The peak of action potentials is artificially set in simulations to $v_p = 30\ mV$ (McDermott et al., 2003; Magee, 1998), whereas the refractory period for neuronal action potential generation is fixed at $\tau_r = 2$ ms (McDermott et al., 2003; Gasparini et al., 2004; Rauch et al., 2003).

B.6 Postsynaptic currents

AMPA receptor-mediated EPSCs recorded at central synapses are characterized by small rise time constants (τ_N^r), namely in between 0.2–0.6 ms (Spruston et al., 1995; Magee and Cook, 2000; Andrásfalvy and Magee, 2001; McDermott et al., 2006), and decay time constants (τ_N) in the range of 2.7–11.6 ms (Andrásfalvy and Magee, 2001; Pankratov and Krishtal, 2003; Smith et al., 2003; McDermott et al., 2006). Furthermore, whole-cell recordings of EPSCs for quantal-like glutamatergic stimulation report amplitudes for these currents generally within ∼15.5–30 pA (Pankratov and Krishtal, 2003; McDermott et al., 2006), and corresponding somatic depolarizations (EPSPs) similarly are in a wide range of values comprised between ∼0.5–7.2 mV, consistent with large quantal size variability of glutamate release from presynaptic terminals (Loebel et al., 2009). Accordingly, in the simulations of Figure 5 we set $\tau_N^r = 0.5$ ms and $\tau_N = 10$ ms and take the two scaling factors $\hat{J}_S$, $\hat{I}_S$ in equation 17 such that (Abbott, 2002)

$$\hat{J}_S = \frac{J_S}{\varrho_c\, Y_T\, \tau_N} \tag{29}$$

$$\hat{I}_S = I_S \left(\frac{1}{\tau_N} - \frac{1}{\tau_N^r}\right) \left(\left(\frac{\tau_N^r}{\tau_N}\right)^{\left(\frac{\tau_N}{\tau_N - \tau_N^r}\right)} - \left(\frac{\tau_N^r}{\tau_N}\right)^{\left(\frac{\tau_N^r}{\tau_N - \tau_N^r}\right)}\right)^{-1} \tag{30}$$

In this fashion, with 3/4 of released neurotransmitter reaching postsynaptic receptors (i.e. $\zeta = 0.75$), setting $J_S = 4.27$ results in EPSP amplitudes approximately equal to I_S. In order to convert PSCs and SICs from voltage to current units, we divide them by typical neuronal input resistance (R_{in}) values which are generally reported in the range of ∼60–150 MΩ (Magee, 1998; McDermott et al., 2006; Routh et al., 2009).

B.7 Slow-inward currents

Astrocyte-mediated SICs are documented in a wide range of amplitudes that spans from >10 pA (Fellin et al., 2004; Perea and Araque, 2005; Chen et al., 2012; Perea et al., 2014; Martín et al., 2015) to >200 pA (Fellin et al., 2004; Kang et al., 2005; Bardoni et al., 2010; Nie et al., 2010), although their majority is mostly found between 30–80 pA in physiological conditions (Fellin et al., 2004; Martín et al., 2015). SICs kinetics also likely varies depending on subunit composition of SIC-mediating NMDA receptors (Traynelis et al., 2010). In general, assuming NR2B-containing NMDARs as the main receptor type mediating SICs (Papouin and Oliet, 2014), mean SICs rise and decay times are respectively reported in ∼30–90 ms and ∼100–800 (Angulo et al., 2004; Fellin et al., 2004). Accordingly, in the simulations of Figure 5 we set $\tau_S^r = 30$ ms and $\tau_N = 600$ ms and take the two scaling factors $\hat{J}_S$, $\hat{I}_S$ in equation 13 such that

$$\hat{J}_A = \frac{J_A}{\varrho_e\, G_T\, \tau_S} \tag{31}$$

$$\hat{I}_A = I_A \left(\frac{1}{\tau_S} - \frac{1}{\tau_S^r}\right) \left(\left(\frac{\tau_S^r}{\tau_S}\right)^{\left(\frac{\tau_N}{\tau_N - \tau_S^r}\right)} - \left(\frac{\tau_S^r}{\tau_S}\right)^{\left(\frac{\tau_S^r}{\tau_S - \tau_S^r}\right)}\right)^{-1} \tag{32}$$

In this fashion, we ultimately choose the value of J_S to account for SIC-mediated depolarizations approximately equal to I_A. As SIC amplitudes are generally reported in terms of current rather than voltage units, we estimate somatic depolarizations ensuing from SICs by expressing these latter in terms of typical EPSCs. Thus, for example, for individual EPSCs of 30 pA that generate 2 mV EPSPs, realistic SICs could be regarded on average to be ∼1–5-fold these EPSCs and thus contribute to a similar extent to 1–5 times typical EPSPs, that is ∼2–10 mV.

B.8 Spike-timing–dependent plasticity

We consider the set of parameters for the nonlinear Ca^{2+} model by Graupner and Brunel (2012, Figure S6) originally proposed by these authors to qualitatively reproduce the classic STDP curve (Bi and Poo, 1998). In addition, SIC-mediated postsynaptic Ca^{2+} transients are assumed similar to presynaptically-triggered Ca^{2+} transients but with likely longer rise and decay times. Finally, both presynaptically-mediated and SIC-mediated Ca^{2+} transients are rescaled by equations analogous to 29–32 in order to obtain transient peak amplitudes equal to C_{pre} and C_{sic} respectively.

Appendix C Parameter ranges and values

Values of model parameters used in our simulations are summarized in the following table. Blank table entries are for those parameters whose value was either taken from previously published studies (De Pittà et al., 2009a; Graupner and Brunel, 2012; Wallach et al., 2014) or estimated on the basis of other model parameters (see Appendix B). Simulation specific (s.s.) parameter values are instead specified within figure captions.

Symbol	Description	Range	Value	Units
	Synaptic dynamics			
τ_d	Depression time constant	>0.01–2	s.s.	s
τ_f	Facilitation time constant	>0.5–2	s.s.	s
U_0	Resting synaptic release probability	<0.09–0.9	s.s.	–
	Neurotransmitter release and time course			
Y_T	Total vesicular glutamate concentration	300–1000	500	mM
ϱ_c	Vescicular vs. mixing volume ratio		0.005	–
τ_c	Glutamate clearance time const.	2–100	25	ms
ζ	Efficacy of synaptic transmission	0–1	0.75	–
	Astrocyte GPCR kinetics			
O_A	Agonist binding rate		0.3	$\mu\mathrm{M}^{-1}\mathrm{s}^{-1}$
τ_A	Agonist unbinding time		0.55	s
	IP_3R kinetics			
O_2	Inact. Ca^{2+} binding rate (with Ca^{2+} act.)	0.04–0.18	0.2	$\mu\mathrm{M}^{-1}\mathrm{s}^{-1}$
d_1	IP_3 binding affinity	0.1–0.15	0.13	μM
d_2	Inact. Ca^{2+} binding affinity (Ca^{2+} act.)		1.05	μM
d_3	IP_3 binding affinity (Ca^{2+} inact.)		0.9434	μM
d_5	Act. Ca^{2+} binding affinity		0.08	μM
	Calcium fluxes			
ϱ_A	ER-to-cytoplasm volume ratio	0.4–0.7	0.18	–
C_T	Total ER Ca^{2+} content	3–5	2	μM
Ω_L	Max. Ca^{2+} leak rate	0.05–0.1	0.1	s^{-1}
Ω_C	Max. Ca^{2+} release rate by IP_3Rs	>6	6	s^{-1}
K_P	Ca^{2+} affinity of SERCA pumps	0.05–0.1	0.05	μM
O_P	Max. Ca^{2+} uptake rate	0.4–1.3	0.9	$\mu\mathrm{M}\,\mathrm{s}^{-1}$
	IP_3 production			
O_β	Max. rate of IP_3 production by PLCβ	0.05–2	1	$\mu\mathrm{M}\,\mathrm{s}^{-1}$
K_δ	Ca^{2+} affinity of PLCδ	0.1–1	0.5	μM
κ_δ	Inhibiting IP_3 affinity of PLCδ	1–1.5	1	μM
O_δ	Max. rate of IP_3 production by PLCδ	<0.8	0.05	$\mu\mathrm{M}\,\mathrm{s}^{-1}$
	IP_3 degradation			
Ω_{5P}	Max. rate of IP_3 degradation by IP-5P	>0.05–0.25	0.1	s^{-1}
K_D	Ca^{2+} affinity of IP_3-3K	0.4–0.5	0.5	μM
K_{3K}	IP_3 affinity of IP_3-3K	0.7–1	1	μM
O_{3K}	Max. rate of IP_3 degradation by IP_3-3K	>0.6	4.5	$\mu\mathrm{M}\,\mathrm{s}^{-1}$
	Gliotransmitter release and time course			
C_θ	Ca^{2+} threshold for exocytosis	0.15–0.8	0.5	μM
τ_G	Glutamate recycling time const.	0.003–1.5	1.66	s
U_A	Resting glutamate release probability	<0.9	0.6	–
ϱ_e	Vescicular vs. mixing volume ratio		$6.5 \cdot 10^{-4}$	–

continued on the next page

Table C1: *continued*

Symbol	Description	Range	Value	Units
τ_e	Glutamate clearance time const.	≤300	200	ms
	Presynaptic receptors			
O_P	Activation rate	>0.3	1.5	$\mu M^{-1}s^{-1}$
τ_P	Inactivation time const.	>30–180	120	s
ξ	Gliotransmission type	0–1	s.s.	–
	Postsynaptic neuron			
τ_m	Membrane time constant	20–70	40	ms
τ_r	Refractory period	1–5	2	ms
E_L	Resting potential	-78.2–-54.8	-60	mV
v_θ	Firing threshold	-55–-51	-55	mV
v_r	Reset potential	-58–-53	-57	mV
v_p	Peak AP amplitude	29.8–41.2	30	mV
R_{in}	Input resistance	60–150	s.s.	MΩ
	Postsynaptic currents			
τ_N^r	EPSC rise time	0.4–0.6	0.5	ms
τ_N	EPSC decay time	2.7–11.6	10	ms
J_S	Synaptic efficacy		4.3	–
I_S	EPSP amplitude	0.5–7.5	2	mV
	Slow inward currents			
τ_S^r	SIC rise time	20–70	20	ms
τ_S	SIC decay time	100–800	600	ms
J_A	SIC efficacy		68	–
I_A	SIC amplitude	1–10	4.5	mV
	Spike-timing dependent plasticity			
C_{pre}	NMDAR-mediated Ca^{2+} increase per AP		1.0	–
τ_{pre}^r	NMDAR Ca^{2+} rise time		10	ms
τ_{pre}	NMDAR Ca^{2+} decay time		30	ms
W_N	Synaptic weight		39.7	–
C_{post}	VDCC-mediated Ca^{2+} increase per AP		2.5	–
τ_{post}^r	VDCC Ca^{2+} rise time		2	ms
τ_{post}	VDCC Ca^{2+} decay time		12	ms
C_{sic}	SIC-mediated Ca^{2+} increase per AP		1.0	–
τ_{sic}^r	SIC Ca^{2+} rise time		5	ms
τ_{sic}	SIC Ca^{2+} decay time		100	ms
W_A	SIC weight		10.6	–
η	Amplification of NMDAR-mediated Ca^{2+}		4	–
θ_d	LTD threshold		1.0	–
θ_p	LTP threshold		2.2	–
γ_d	LTD learning rate		0.57	s^{-1}
γ_p	LTP learning rate		2.32	s^{-1}
$\rho_\star$	Boundary between UP/DOWN states		0.5	–
τ_ρ	Decay time of synaptic change		1.5	s
σ	Noise amplitude		0.1	–
β	Fraction of synapses in the DOWN state		0.5	–
b	UP/DOWN Synaptic strength ratio		4	–

1 Figure Captions

Figure 1. Pathways of glutamatergic gliotransmission. Perisynaptic astrocytic processes in several brain areas and different excitatory (but also inhibitory) synapses, may release glutamate in a Ca^{2+}-dependent fashion. In turn, released astrocytic glutamate, may increase (or decrease) synaptic neurotransmitter release by activating extrasynaptically-located presynaptic receptors (*magenta arrows*), or contribute to postsynaptic neuronal depolarization by binding to extrasynaptic NMDA receptors (*orange arrows*) which mediate slow inward currents (SICs). These receptors often (but not always) contain NR2B subunits and are thus different with respect to postsynaptic NMDARs. Glutamate release by the astrocyte could be triggered either by activity from the same synapses that are regulated by the astrocyte (homosynaptic scenario) or by other synapses that are not directly reached by glutamatergic gliotransmission (heterosynaptic scenario).

Figure 2. Biophysical modeling of a gliotransmitter-regulated synapse. **A-C** Model of synaptic release. Incoming presynaptic spikes (**A**) increase intrasynaptic Ca^{2+} levels which directly control the probability of release of available neurotransmitter resources (**B**, Nt. Rel. Pr.) and decrease, upon release, the fraction (or probability) of neurotransmitter-containing vesicles available for release (Avail. Nt. Pr.). Each spike ensues in release of a quantum of neurotransmitter from the synapse (**C**, Released Nt.) whose concentration in the perisynaptic space decays exponentially. Synapse parameters: $\tau_d = 0.5$ s, $\tau_f = 0.3$ s, $U_0 = 0.6$. Stimulation by Poisson-distributed APs with an average rate of 5 Hz. **D-F** Model for astrocyte activation. Synaptically-released neurotransmitter in the perisynaptic space (**D**) binds astrocytic receptors (**E**, Bound Ast. Rec.), resulting in IP_3 production which triggers Ca^{2+} signalling in the astrocyte (**F**). This latter also depends on the fraction of deinactivated IP_3 receptors/Ca^{2+} channels (Deinact. IP_3Rs) on the astrocyte ER membrane (see Appendix A.1). **G-I** Model for gliotransmitter release. The increase of astrocytic Ca^{2+} beyond a threshold concentration (**G**, *cyan dashed line*) results in the release of a quantum of gliotransmitter, which decreases the probability of further release of gliotransmitter (**H**, Avail. Gt. Pr.) while transiently increasing extracellular gliotransmitter concentration (**I**, Released Gt.). Model parameters as in the Table of Appendix C.

Figure 3. Presynaptic pathway of gliotransmission. Gliotransmitter released from the astrocyte (**A**) binds extrasynaptically-located presynaptic receptors (**B**) thereby decreasing or increasing synaptic release depending on the type of gliotransmitter and receptor. In the release-decreasing case, synaptic release probability could approach zero by gliotransmission (**C**, *red trace*, $\xi = 0$), although in practice, less dramatic reductions are more likely to be measured with respect to the original value in the absence of gliotransmission (*black dashed line*). The reduction in synaptic release probability, changes pair pulse plasticity increasing the pair pulse ratio (**D**). In the case of release-increasing gliotransmission, synaptic release probability could instead increase up to one (**E**, *green trace*, $\xi = 1$). In turn, pair pulse plasticity changes towards a decrease of the ensuing pair pulse ratio (**F**). Parameters as in Appendix C Table except for $\varrho_e = 10^{-4}$, $O_P = 0.6\ \mu\mathrm{M}^{-1}\,\mathrm{s}^{-1}$, $\tau_P = 30$ s, $\zeta = 0.54$, $J_S = 3$ mV, $R_{in} = 60$ MΩ.

Figure 4. Gliotransmitter-mediated modulation of synaptic frequency response. Decrease (**A**) or increase (**D**) of synaptic release probability by gliotransmission modulate the average per-spike synaptic release, resulting in a change of the synapse frequency response. Monotonically-decreasing frequency responses, that are typical of depressing synapses could be flattened by release-decreasing gliotransmission (**B**, *black* vs. *red points*), and vice-versa, almost non-

monotonic ones, characteristic of facilitating synapses, could turn into monotonically-decreasing responses by release-increasing gliotransmission (**E**, *black* vs. *green points*). Changes in frequency response depend on whether gliotransmission impinges on the very synapse that is triggered by (homosynaptic/closed-loop scenario) or not (heterosynaptic/open-loop scenario). In the homosynaptic scenario, the synaptic response is expected to change only for presynaptic firing rates that are sufficiently high to trigger gliotransmitter release from the astrocyte (**B**, **E**, *cyan points*). Data points and error bars: mean $\pm$ STD for $n = 20$ (no gliot. and heterosyn. gliot.) or $n = 200$ simulations (homosyn. gliot.) with 60 s-long Poisson-distributed presynaptic spike trains. **C**, **F** The change of synaptic frequency response mediated by gliotransmission (three consecutive gliotransmitter releases at the time instants marked by *triangles*) leads to changes in how presynaptic firing rates (*top panels*) are transmitted by the synapse (*bottom panels*). Simulated postsynaptic currents (PSC) are shown as average traces of $n = 1000$ simulations for gliotransmitter release at 1 Hz. Release-decreasing gliotransmission was achieved for $\xi = 0$, whereas $\xi = 1$ was used for release-increasing gliotransmission. Depressing synapse in **A**, **B**: $\tau_d = 0.5$ s, $\tau_f = 0.3$ s, $U_0 = 0.6$; facilitating synapse in **D**, **E**: $\tau_d = 0.5$ s, $\tau_f = 0.5$ s, $U_0 = 0.15$. Other model parameters as in Figure 3 except for $R_{in} = 300$ MΩ.

Figure 5. Postsynaptic pathway of gliotransmission by slow inward currents. The transient increase of gliotransmitter concentration in the perisynaptic space (**A**), triggers a slow inward (depolarizing) current (SIC) in the postsynaptic neuron (**B**, **C**). Such SIC adds to postsynaptic currents triggered by presynaptic spikes (**D**, **E**, *cyan triangle* marks gliotransmitter release/SIC onset) and may dramatically alter postsynaptic firing (**F**). In general postsynaptic firing frequency increases both with SIC amplitude (**G**) and frequency (**H**). In this latter case however, SICs as ample as 30 pA (similar to what reported in several experiments) need to impinge on the postsynaptic neuron at unrealistically high rates ($\gg$0.1 Hz) in order to trigger a sensible change in the neuron's firing rate (*black data points*). Lower, more realistic SIC rates may affect neuronal firing only for larger SIC amplitudes (e.g. 45 pA, *grey data points*). The entity of SIC-mediated increase of postsynaptic neuronal firing further depends on the neuron's state of depolarization at SIC timings which is set by synaptic inputs (*blue* and *cyan data points*). Data points and error bars: mean $\pm$ STD out of $n = 50$ simulations with presynaptic Poisson-distributed spike trains. Parameters as in Appendix C Table except for $\varrho_e = 10^{-4}$, $\tau_e = 200$ ms, $\tau_S^r = 10$ ms, $R_{in} = 150$ MΩ.

Figure 6. STDP Modulation by gliotransmitter regulation of synaptic release. (**A**, **B**) Rationale of LTD and LTP without (**A.1**, **B.1**) and with either release-decreasing (**A.2**, **B.2**, $\xi = 0$) or release-increasing gliotransmission (**A.3**, **B.3**, $\xi = 1$) setting on at the *red/green marks*. **C** Percentage of time spent by postsynaptic Ca^{2+} transients (*top panel*) above depression (*dashed lines*) and potentiation thresholds (*solid lines*) for spike timing intervals (Δt) between $\pm$100 ms, and resulting STDP curves (*bottom panel*) in the absence of gliotransmission (no gliot., *black curve*) and with maximal release-decreasing (R.D., *red curve*) or release-increasing gliotransmission (R.I., *green circles*). **D** In general, strength and direction (i.e. "type") of gliotransmission may dramatically modulate STDP. For example, synaptic changes are attenuated when synaptic release is decreased by gliotransmission (area below the *black dashed line*). Conversely, for sufficiently strong release-increasing gliotransmission (area above the *black dashed line*), the LTP window shrinks and LTD may be measured for all $\Delta t < 0$, as well as for sufficiently large $\Delta t > 0$. **E** A closer inspection of STDP curves indeed reveals that LTD (*yellow curve*) increases for larger synaptic release accounted by gliotransmission, while the ratio between areas underneath the LTP and LTD (*magenta curve*), initially in favor of the former (i.e. for release-decreasing gliotransmission), reduces to zero for large enough release-increasing

gliotransmission, when two open LTD windows appear outside a small LTP window center for small $\Delta t > 0$ (*hatched area*). Synaptic parameters: $\tau_d = 0.33$ s, $\tau_f = 0.33$ s, $U = 0.5$ s. Other parameters as in Appendix C Table except for $\varrho_e = 10^{-4}$, $\tau_c = 1$ ms, $W_N = 78.7$, $\tau_P = 5$ s in **A**, **B** and $\tau_P = 30$ s otherwise.

Figure 7. STDP modulation by gliotransmitter-mediated SICs. **A**, **B** Inspection of postsynaptic Ca^{2+} in the initial part of a pairing protocol that includes a gliotransmitter-mediated slow inward current (SIC) arriving to the postsynaptic neuron at $t = 0.1$ s, illustrates how SICs have the potential to modulate postsynaptic Ca^{2+} thereby regulating LTD and LTP. **C** The magnitude of modulation depends on how large SICs are with respect to synaptic inputs (EPSCs) as well as at **D** what rate they occur. **E**, **F** Impact of the delay ($\Delta\varsigma$) at which SICs occur with respect to pre/post pairs. **G** STDP curves as a function of the SIC-pre/post pair delay ($\Delta\varsigma$) show how LTD could get stronger while the LTP window shrink for small-to-intermediate $\Delta\varsigma \leq 0$ in correspondence with **H**, **I** a maximum of the duration of Ca^{2+} transients above the LTD threshold. These results were obtained assuming SIC rise and decay time constants respectively equal to $\tau_s^r = \bar{\tau}_s^r = 20$ ms and $\tau_s = \bar{\tau}_s = 200$ ms. **J**-**L** Peak and range of this LTD increase ultimately depend on SIC kinetics as reflected by the change of sample curves for specific $\Delta\varsigma$ (*yellow curve*) and spike timing intervals (*cyan* and *purple curves*) when SIC rise and/or decay time constants was slowed down 1.5-fold (*orange* and *blue curves* respectively). **C**, **D** STDP curves were calculated for 60 pre/post pairings at 1 Hz and included SICs starting 0.1 s before the first pairing and occurring at 0.1 Hz. The same pairing protocol but with SIC frequency of 0.2 Hz was used instead in figures **G**–**L** although SIC onset and kinetics were varied respectively according to $\Delta\varsigma$, τ_S^r and τ_S. Synaptic parameters: $\tau_d = 0.33$ s, $\tau_f = 0.33$ s, $U_0 = 0.5$ s. Other parameters as in Appendix C Table except for $\varrho_e = 10^{-4}$, $\tau_c = 1$ ms, $\tau_e = 200$ ms, $\tau_S^r = 5$ ms, $\tau_S = 100$ ms.

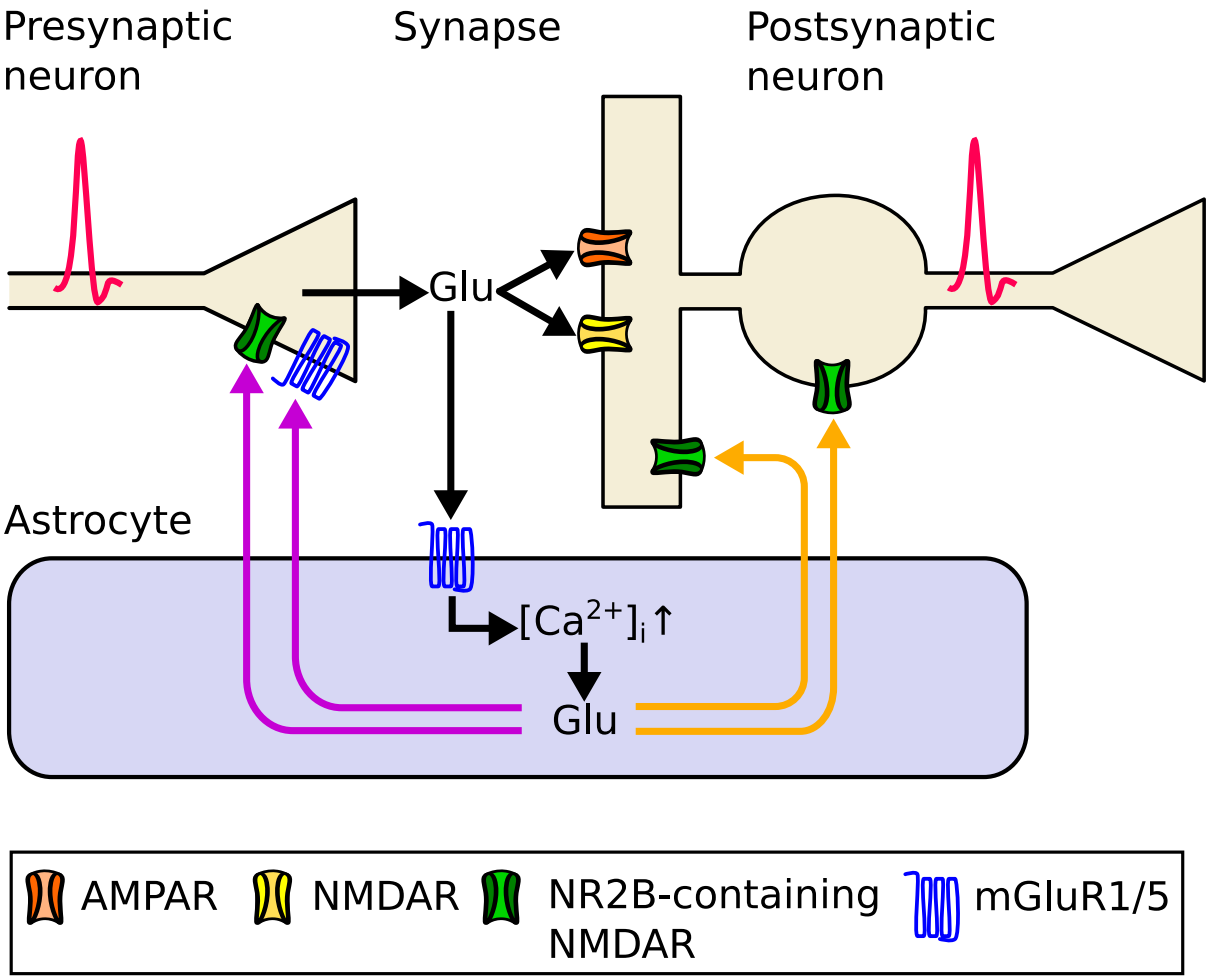

Figure 1: Pathways of glutamatergic gliotransmission.

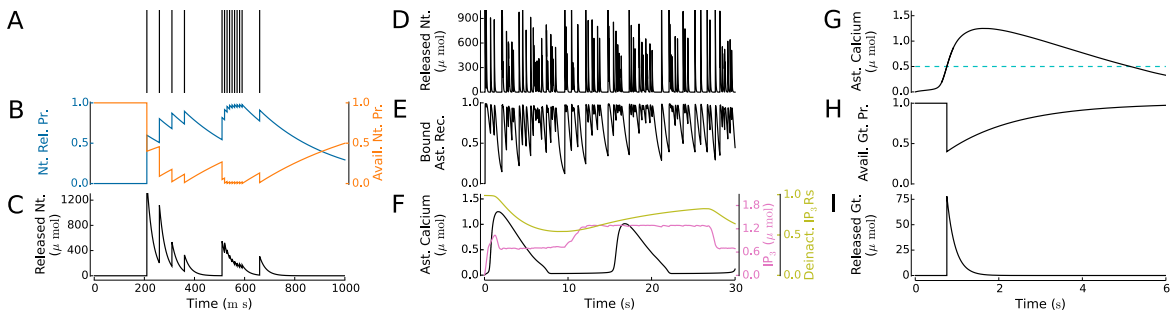

Figure 2: Biophysical modeling of a gliotransmitter-regulated synapse.

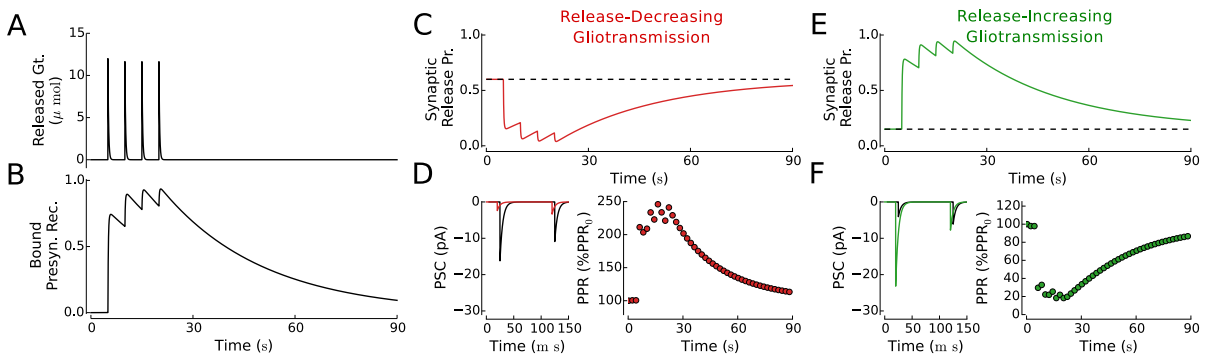

Figure 3: Presynaptic pathway of gliotransmission.

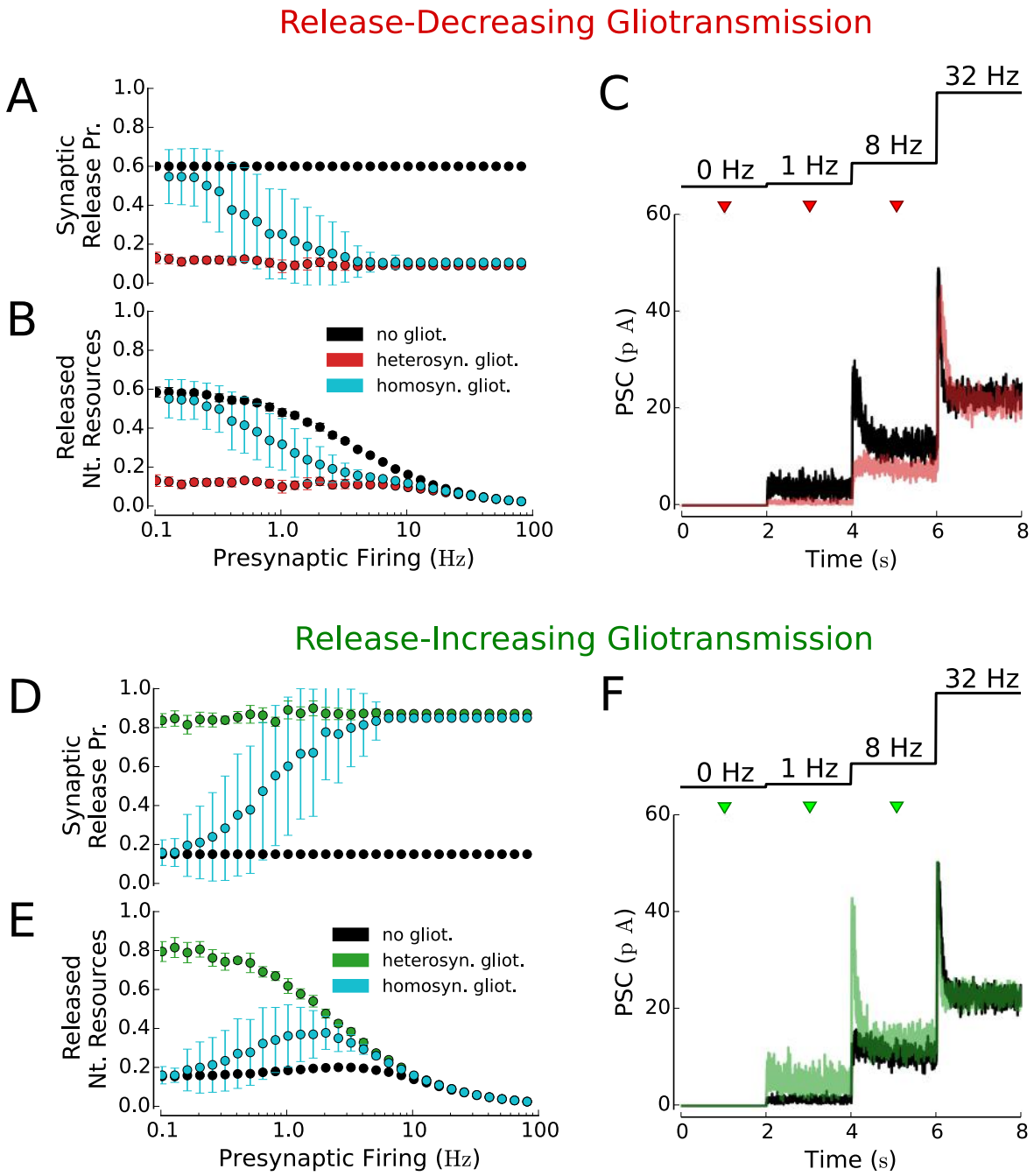

Figure 4: Gliotransmitter-mediated modulation of synaptic frequency response.

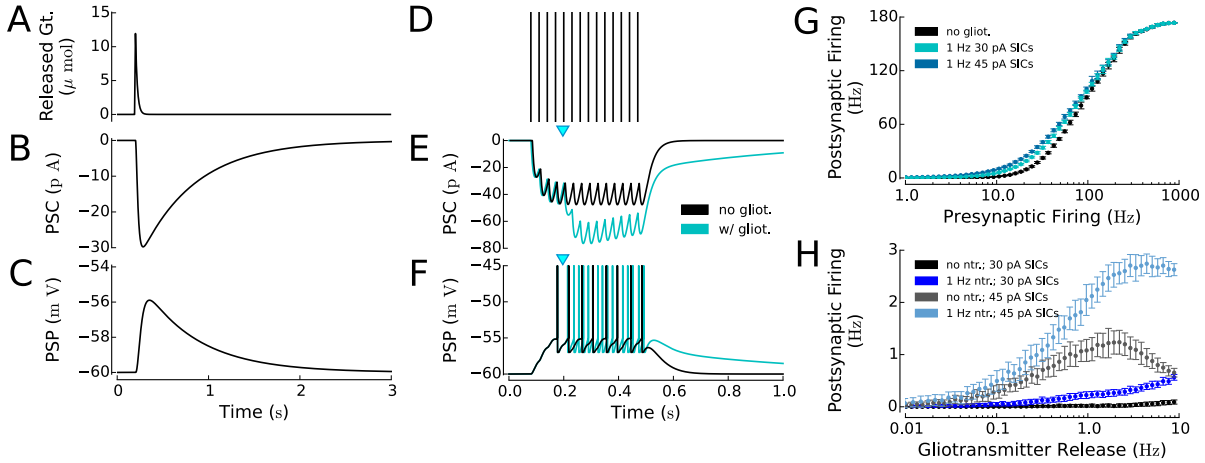

Figure 5: Postsynaptic pathway of gliotransmission by slow inward currents.

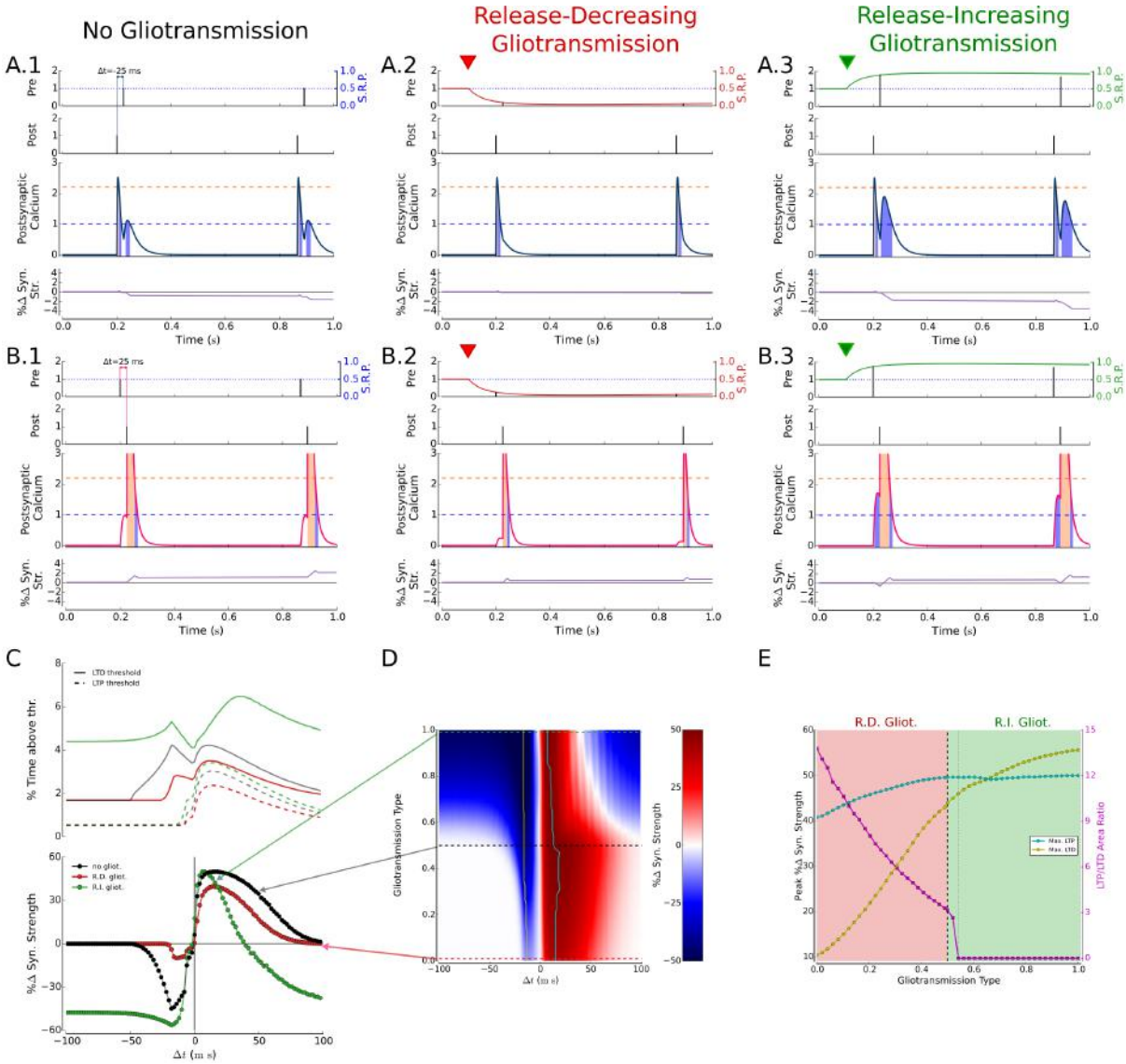

Figure 6: STDP Modulation by gliotransmitter regulation of synaptic release.

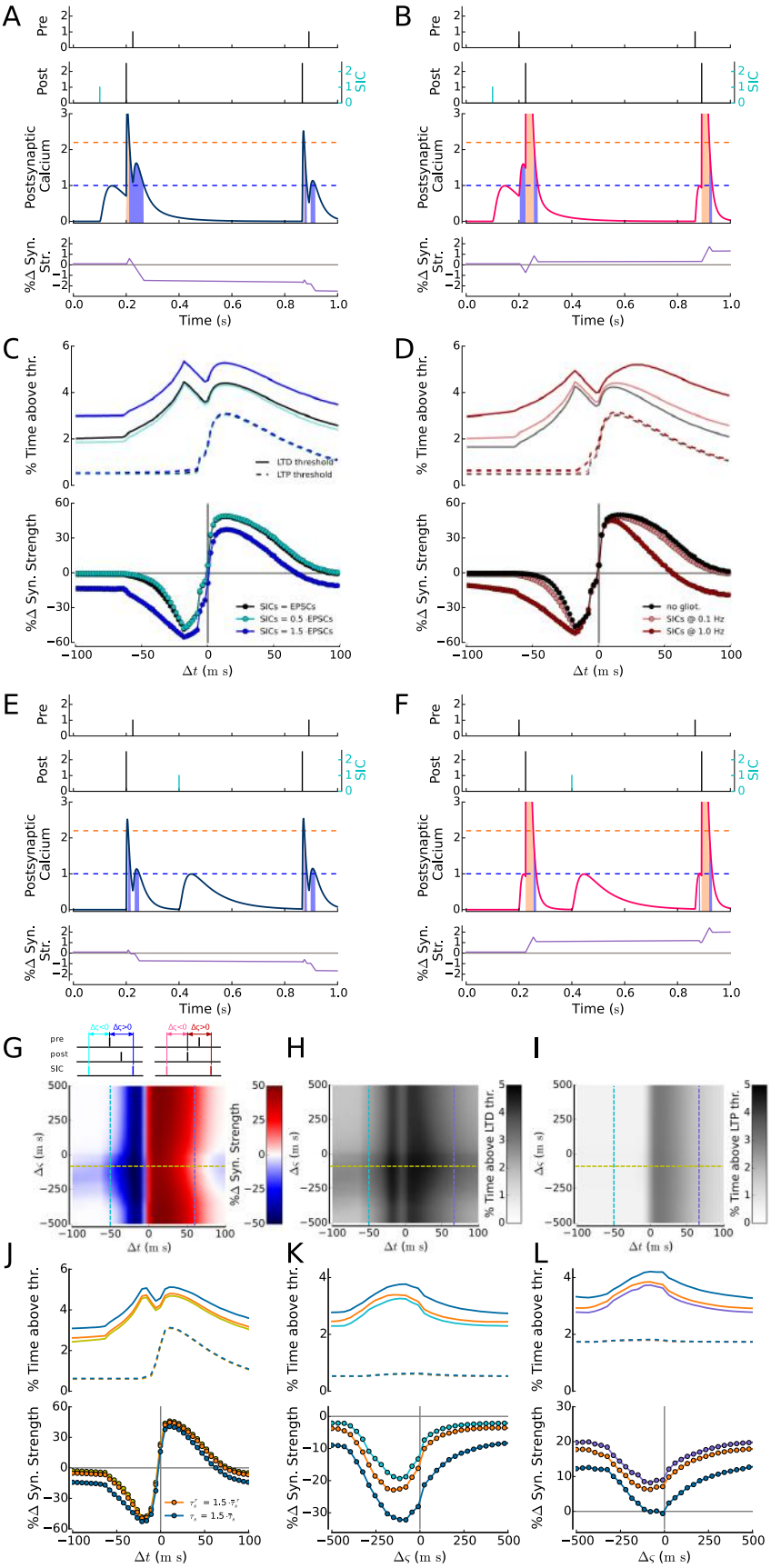

Figure 7: STDP modulation by gliotransmitter-mediated SICs.

References

Abbott, L. F. and Nelson, S. B. (2000). Synaptic plasticity: taming the beast. *Nature*, 3:1178–1183.

Abbott, L. F. and Regehr, W. G. (2004). Synaptic computation. *Nature*, 431:796–803.

Abbott, N. J. (2002). Astrocyte-endothelial interactions and blood-brain barrier permeability. *J. Anat.*, 200:629–638.

Agulhon, C., Petravicz, J., McMullen, A. B., Sweger, E. J., Minton, S. K., Taves, S. R., Casper, K. B., Fiacco, T. A., and McCarthy, K. D. (2008). What is the role of astrocyte calcium in neurophysiology? *Neuron*, 59:932–946.

Andrásfalvy, B. and Magee, J. (2001). Distance-dependent increase in AMPA receptor number in the dendrites of adult hippocampal CA1 pyramidal neurons. *J. Neurosci.*, 21(23):9151–9159.

Angulo, M. C., Kozlov, A. S., Charpak, S., and Audinat, E. (2004). Glutamate released from glial cells synchronizes neuronal activity in the hippocampus. *J. Neurosci.*, 24(31):6920–6927.

Araque, A., Carmignoto, G., Haydon, P. G., Oliet, S. H. R., Robitaille, R., and Volterra, A. (2014). Gliotransmitters travel in time and space. *Neuron*, 81(4):728–739.

Araque, A., Parpura, V., Sanzgiri, R. P., and Haydon, P. G. (1998a). Glutamate-dependent astrocyte modulation of synaptic transmission between cultured hippocampal neurons. *Eur. J. Neurosci.*, 10:2129–2142.

Araque, A., Parpura, V., Sanzgiri, R. P., and Haydon, P. G. (1999). Tripartite synapses: glia, the unacknowledged partner. *Trends Neurosci.*, 23(5):208–215.

Araque, A., Sanzgiri, R. P., Parpura, V., and Haydon, P. G. (1998b). Calcium elevation in astrocytes causes an NMDA receptor-dependent increase in the frequency of miniature synaptic currents in cultured hippocampal neurons. *J. Neurosci.*, 18(17):6822–6829.

Aronica, E., Gorter, J. A., Ijlst-Keizers, H., Rozemuller, A. J., Yankaya, B., Leenstra, S., and Troost, D. (2003). Expression and functional role of mGluR3 and mGluR5 in human astrocytes and glioma cells: opposite regulation of glutamate transporter proteins. *Eur. J. Neurosci.*, 17:2106–2118.

Bains, J. S. and Oliet, S. H. R. (2007). Glia: they make your memories stick! *Trends Neurosci.*, 30(8):417–424.

Banerjee, A., Larsen, R. S., Philpot, B. D., and Paulsen, O. (2015). Roles of presynaptic NMDA receptors in neurotransmission and plasticity. *Trends in Neurosciences*, page in press.

Barbour, B. (2001). An evaluation of synapse independence. *J. Neurosci.*, 21(20):7969–7984.

Barbour, B. and Häusser, M. (1997). Intersynaptic diffusion of neurotransmitter. *Trends Neurosci.*, 20:377–384.

Bardoni, R., Ghirri, A., Zonta, M., Betelli, C., Vitale, G., Ruggieri, V., Sandrini, M., and Carmignoto, G. (2010). Glutamate-mediated astrocyte-to-neuron signalling in the rat dorsal horn. *J. Physiol.*, 588(5):831–846.

Barres, B. (2008). The mystery and magic of glia: a perspective on their roles in health and disease. *Neuron*, 60(3):430–440.

Bazargani, N. and Attwell, D. (2016). Astrocyte calcium signaling: the third wave. *Nature Neuroscience*, 19(2):182–189.

Bender, V. A., Bender, K. J., Brasier, D. J., and Feldman, D. E. (2006). Two coincidence detectors for spike timing-dependent plasticity in somatosensory cortex. *The Journal of neuroscience*, 26(16):4166–4177.

Benedetti, B., Matyash, V., and Kettenmann, H. (2011). Astrocytes control GABAergic inhibition of neurons in the mouse barrel cortex. *J. Physiol.*, 589(5):1159–1172.

Bergersen, L., Morland, C., Ormel, L., Rinholm, J. E., Larsson, M., Wold, J. F. H., Rø e, r. A. T., Stranna, A., Santello, M., Bouvier, D., Ottersen, O. P., Volterra, A., and Gundersen, V. (2012). Immunogold detection of L-glutamate and D-serine in small synaptic-like microvesicles in adult hippocampal astrocytes. *Cereb. Cortex*, 22(7):1690–1697.

Bergersen, L. H. and Gundersen, V. (2009). Morphological evidence for vesicular glutamate release from astrocytes. *Neuroscience*, 158:260–265.

Berridge, M. J., Bootman, M. D., and Roderick, H. L. (2003). Calcium signalling: dynamics, homeostasis and remodelling. *Nat. Rev. Mol. Cell. Biol.*, 4:517–529.

Bezzi, P., Gundersen, V., Galbete, J. L., Seifert, G., Steinhäuser, C., Pilati, E., and Volterra, A. (2004). Astrocytes contain a vesicular compartment that is competent for regulated exocytosis of glutamate. *Nat. Neurosci.*, 7(6):613–620.

Bezzi, P. and Volterra, A. (2001). A neuron-glia signalling network in the active brain. *Curr. Opinion Neurobiol.*, 11:387–394.

Bi, G. and Poo, M. (1998). Synaptic modifications in cultured hippocampal neurons: dependence on spike timing, synaptic strength, and postsynaptic cell type. *The Journal of Neuroscience*, 18(24):10464–10472.

Bi, G.-Q. and Poo, M.-M. (2001). Synaptic modeification by correlated activity: Hebb's postulate revisited. *Annu. Rev. Neurosci.*, 24:139–66.

Bloodgood, B. L. and Sabatini, B. L. (2007). Ca^{2+} signaling in dendritic spines. *Current opinion in neurobiology*, 17(3):345–351.

Bonansco, C., Couve, A., Perea, G., Ferradas, C. A., Roncagliolo, M., and Fuenzalida, M. (2011). Glutamate released spontaneously from astrocytes sets the threshold for synaptic plasticity. *Eur. J. Neurosci.*, 33:1483–1492.

Bowser, D. N. and Khakh, B. S. (2007). Two forms of single-vesicle astrocyte exocytosis imaged with total internal reflection fluorescence microscopy. *Proc. Natl. Acad. Sci. USA*, 104(10):4212–4217.

Brabet, I., Mary, S., Bockaert, J., and Pin, J. (1995). Phenylglycine derivatives discriminate between mGluR1- and mGluR5-mediated responses. *Neuropharmacology*, 34(8):895–903.

Brody, D. L. and Yue, D. T. (2000). Release-independent short-term synaptic depression in cultured hippocampal neurons. *J. Neurosci.*, 20(7):2480–2494.

Buchanan, K. A. and Mellor, J. R. (2007). The development of synaptic plasticity induction rules and the requirement for postsynaptic spikes in rat hippocampal CA1 pyramidal neurones. *The Journal of Physiology*, 585(2):429–445.

Buchanan, K. A. and Mellor, J. R. (2010). The activity requirements for spike timing-dependent plasticity in the hippocampus. *Frontiers in Synaptic Neuroscience*, 2(11):1–5.

Burkitt, A. N. (2006). A review of the integrate-and-fire neuron model: I. Homogeneous synaptic input. *Biol. Cybern.*, 95(1):1–19.

Cai, Y., Gavornik, J. P., Cooper, L. N., Yeung, L. C., and Shouval, H. Z. (2007). Effect of stochastic synaptic and dendritic dynamics on synaptic plasticity in visual cortex and hippocampus. *Journal of Neurophysiology*, 97(1):375–386.

Campanac, E. and Debanne, D. (2008). Spike timing-dependent plasticity: a learning rule for dendritic integration in rat CA1 pyramidal neurons. *The Journal of Physiology*, 586(3):779–793.

Caporale, N. and Dan, Y. (2008). Spike timing-dependent plasticity: a hebbian learning rule. *Annu. Rev. Neurosci.*, 31:25–46.

Chen, N., Sugihara, H., Sharma, J., Perea, G., Petravicz, J., Le, C., and Sur, M. (2012). Nucleus basalis enabled stimulus specific plasticity in the visual cortex is mediated by astrocytes. *Proc. Natl. Acad. Sci. USA*, 109(41):E2832E2841.

Chen, X., Wang, L., Zhou, Y., Zheng, L.-H., and Zhou, Z. (2005). "Kiss-and-run" glutamate secretion in cultured and freshly isolated rat hippocampal astrocytes. *J. Neurosci.*, 25(40):9236–9243.

Clements, J. D. (1996). Transmitter timecourse in the synaptic cleft: its role in central synaptic function. *Trends Neurosci.*, 19(5):163–171.

Clements, J. D., Lester, R. A. J., Tong, G., Jahr, C. E., and Westbrook, G. L. (1992). The time course of glutamate in the synaptic cleft. *Science*, 258:1498–1501.

Crippa, D., Schenk, U., Francolini, M., Rosa, P., Verderio, C., Zonta, M., Pozzan, T., Matteoli, M., and Carmignoto, G. (2006). Synaptobrevin2-expressing vesicles in rat astrocytes: insights into molecular characterization, dynamics and exocytosis. *J. Physiol.*, 570(3):567–582.

Cull-Candy, S., Brickley, S., and Farrant, M. (2001). NMDA receptor subunits: diversity, development and disease. *Curr. Opin. Neurobiol.*, 11(3):327–335.

Daggett, L., Sacaan, A., Akong, M., Rao, S., Hess, S., Liaw, C., Urrutia, A., Jachec, C., Ellis, S., Dreessen, J., et al. (1995). Molecular and functional characterization of recombinant human metabotropic glutamate receptor subtype 5. *Neuropharmacology*, 34(8):871–886.

Danbolt, N. C. (2001). Glutamate uptake. *Progress Neurobiol.*, 65:1–105.

D'Ascenzo, M., Fellin, T., Terunuma, M., Revilla-Sanchez, R., Meaney, D., Auberson, Y., Moss, S., and Haydon, P. (2007). mGluR5 stimulates gliotransmission in the nucleus accumbens. *Proc. Natl. Acad. Sci. USA*, 104(6):1995.

De Pittà, M., Brunel, N., and Volterra, A. (2015). Astrocytes: orchestrating synaptic plasticity? *Neuroscience*.

De Pittà, M., Goldberg, M., Volman, V., Berry, H., and Ben-Jacob, E. (2009a). Glutamate-dependent intracellular calcium and IP_3 oscillating and pulsating dynamics in astrocytes. *J. Biol. Phys.*, 35:383–411.

De Pittà, M., Volman, V., Berry, H., and Ben-Jacob, E. (2011). A tale of two stories: astrocyte regulation of synaptic depression and facilitation. *PLoS Comput. Biol.*, 7(12):e1002293.

De Pittà, M., Volman, V., Berry, H., Parpura, V., Liaudet, N., Volterra, A., and Ben-Jacob, E. (2013). Computational quest for understanding the role of astrocyte signaling in synaptic transmission and plasticity. *Front. Comp. Neurosci.*, 6:98.

De Pittà, M., Volman, V., Levine, H., and Ben-Jacob, E. (2009b). Multimodal encoding in a simplified model of intracellular calcium signaling. *Cogn. Proc.*, 10(S1):55–70.

De Young, G. W. and Keizer, J. (1992). A single-pool inositol 1,4,5-trisphosphate-receptor-based model for agonist-stimulated oscillations in Ca^{2+} concentration. *Proc. Natl. Acad. Sci. USA*, 89:9895–9899.

Del Castillo, J. and Katz, B. (1954). Quantal components of the end-plate potential. *J. Physiol.*, 124:560–573.

Destexhe, A., Mainen, Z. F., and Sejnowski, T. J. (1994). Synthesis of models for excitable membranes, synaptic transmission and neuromodulation using a common kinetic formalism. *J. Comput. Neurosci.*, 1:195–230.

Di Castro, M., Chuquet, J., Liaudet, N., Bhaukaurally, K., Santello, M., Bouvier, D., Tiret, P., and Volterra, A. (2011). Local Ca^{2+} detection and modulation of synaptic release by astrocytes. *Nat. Neurosci.*, 14:12761284.

Diamond, J. S. (2005). Deriving the glutamate clearance time course from transporter currents in CA1 hippocampal astrocytes: transmitter uptake gets faster during development. *J. Neurosci.*, 25(11):2906 2916.

Ding, S., Fellin, T., Zhu, Y., Lee, S., Auberson, Y. P., Meaney, D. F., Coulter, D. A., Carmignoto, G., and Haydon, P. G. (2007). Enhanced astrocytic Ca^2+ signals contribute to neuronal excitotoxicity after status epilepticus. *The Journal of Neuroscience*, 27(40):10674–10684.

Dittman, J. S., Kreitzer, A. C., and Regehr, W. G. (2000). Interplay between facilitation, depression, and residual calcium at three presynaptic terminals. *J. Neurosci.*, 20(4):1374–1385.

Domercq, M., Brambilla, L., Pilati, E., Marchaland, J., Volterra, A., and Bezzi, P. (2006). P2Y1 receptor-evoked glutamate exocytosis from astrocytes: control by tumor necrosis factor-α and prostaglandins. *J. Biol. Chem.*, 281:30684–30696.

Emptage, N. J., Reid, C. A., and Fine, A. (2001). Calcium stores in hippocampal synaptic boutons mediate short-term plasticity, store-operated Ca^{2+} entry, and spontaneous transmitter release. *Neuron*, 29:197–208.

Evans, R. C. and Blackwell, K. T. (2015). Calcium: amplitude, duration, or location? *The Biological Bulletin*, 228(1):75–83.

Fellin, T., Gonzalo, M. G., Gobbo, S., Carmignoto, G., and Haydon, P. G. (2006). Astrocytic glutamate is not necessary for the generation of epileptiform neuronal activity in hippocampal slices. *J. Neurosci.*, 26(36):9312–9322.

Fellin, T., Pascual, O., Gobbo, S., Pozzan, T., Haydon, P. G., and Carmignoto, G. (2004). Neuronal synchrony mediated by astrocytic glutamate through activation of extrasynaptic NMDA receptors. *Neuron*, 43:729–743.

Fiacco, T. A. and McCarthy, K. D. (2004). Intracellular astrocyte calcium waves *in situ* increase the frequency of spontaneous AMPA receptor currents in CA1 pyramidal neurons. *J. Neurosci.*, 24(3):722–732.

Fortune, E. S. and Rose, G. J. (2001). Short-term synaptic plasticity as a temporal filter. *Trends Neurosci.*, 24(7):381–385.

Fourcaud, N. and Brunel, N. (2002). Dynamics of the firing probability of noisy integrate-and-fire neurons. *Neural Comput.*, 14(9):2057–2110.

Froemke, R. C. and Dan, Y. (2002). Spike-timing-dependent synaptic modification induced by natural spike trains. *Nature*, 416(6879):433–438.

Froemke, R. C., Debanne, D., and Bi, G. (2010). Temporal modulation of spike-timing-dependent plasticity. *Frontiers in synaptic neuroscience*, 2(19):1–16.

Froemke, R. C., Tsay, I. A., Raad, M., Long, J. D., and Dan, Y. (2006). Contribution of individual spikes in burst-induced long-term synaptic modification. *Journal of Neurophysiology*, 95(3):1620–1629.

Gasparini, S. and Magee, J. (2006). State-dependent dendritic computation in hippocampal CA1 pyramidal neurons. *J. Neurosci.*, 26(7):2088–2100.

Gasparini, S., Migliore, M., and Magee, J. (2004). On the initiation and propagation of dendritic spikes in CA1 pyramidal neurons. *J. Neurosci.*, 24(49):11046–11056.

Gerstner, W. and Kistler, W. M. (2002). Mathematical formulations of Hebbian learning. *Biological Cybernetics*, 87(5-6):404–415.

Golding, N., Staff, N., and Spruston, N. (2002). Dendritic spikes as a mechanism for cooperative long-term potentiation. *Nature*, 418(6895):326–331.

Graupner, M. and Brunel, N. (2010). Mechanisms of induction and maintenance of spike-timing dependent plasticity in biophysical synapse models. *Frontiers in Computational Neuroscience*, 4(136):1–19.

Graupner, M. and Brunel, N. (2012). Calcium-based plasticity model explains sensitivity of synaptic changes to spike pattern, rate, and dendritic location. *Proc. Natl. Acad. Sci. USA*, page Online.

Halassa, M. and Haydon, P. (2010). Integrated brain circuits: astrocytic networks modulate neuronal activity and behavior. *Annu. Rev. Physiol.*, 72:335–355.

Halassa, M. M., Fellin, T., and Haydon, P. G. (2007a). The tripartite synapse: roles for gliotransmission in health and disease. *Trends in Molecular Medicine*, 13(2):54–63.

Halassa, M. M., Fellin, T., Takano, H., Dong, J.-H., and Haydon, P. G. (2007b). Synaptic islands defined by the territory of a single astrocyte. *J. Neurosci.*, 27(24):6473–6477.

Hamilton, N. B. and Attwell, D. (2010). Do astrocytes really exocytose neurotransmitters? *Nature Reviews Neuroscience*, 11(4):227–238.

Harris, K. M. and Sultan, P. (1995). Variation in the number, location and size of synaptic vesicle provides an anatomical basis for the nonuniform probability of release at hippocampal CA1 synapses. *Neuropharmacology*, 34(11):1387–1395.

Haydon, P. G. (2001). Glia: listening and talking to the synapse. *Nat. Rev. Neurosci.*, 2:185–193.

Hebb, D. O. (1949). *The organization of behavior; a neuropsychological theory.* J. Wiley, New York.

Herman, M. A. and Jahr, C. E. (2007). Extracellular glutamate concentration in hippocampal slice. *J. Neurosci.*, 27(36):9736–9741.

Hirase, H., Qian, L., Barthó, P., and Buzsáki, G. (2004). Calcium dynamics of cortical astrocytic networks *in vivo*. *PLoS Biol.*, 2(4):0494–0496.

Hromádka, T., DeWeese, M. R., and Zador, A. M. (2008). Sparse representation of sounds in the unanesthetized auditory cortex. *PLoS Biol.*, 6(1):e16.

Innocenti, B., Parpura, V., and Haydon, P. G. (2000). Imaging extracellular waves of glutamate during calcium signaling in cultured astrocytes. *J. Neurosci.*, 20:1800–1808.

Ismailov, I., Kalikulov, D., Inoue, T., and Friedlander, M. J. (2004). The kinetic profile of intracellular calcium predicts long-term potentiation and long-term depression. *The Journal of Neuroscience*, 24(44):9847–9861.

Jahr, C. E. and Stevens, C. F. (1990). Voltage dependence of NMDA-activated macroscopic conductances predicted by single-channel kinetics. *J. Neurosci.*, 10(9):3178–3182.

Jourdain, P., Bergersen, L. H., Bhaukaurally, K., Bezzi, P., Santello, M., Domercq, M., Matute, C., Tonello, F., Gundersen, V., and Volterra, A. (2007). Glutamate exocytosis from astrocytes controls synaptic strength. *Nat. Neurosci.*, 10(3):331–339.

Kang, J., Jiang, L., Goldman, S. A., and Nedergaard, M. (1998). Astrocyte-mediated potentiation of inhibitory synaptic transmission. *Nat. Neurosci.*, 1(8):683–692.

Kang, M. and Othmer, H. (2009). Spatiotemporal characteristics of calcium dynamics in astrocytes. *Chaos*, 19(3):037116.

Kang, N., Xu, J., Xu, Q., Nedergaard, M., and Kang, J. (2005). Astrocytic glutamate release-induced transient depolarization and epileptiform discharges in hippocampal CA1 pyramidal neurons. *J. Neurophysiol.*, 94:4121–4130.

Kreft, M., Stenovec, M., Rupnik, M., Grilc, S., Kržan, M., Potokar, M., Pangršič, T., Haydon, P. G., and Zorec, R. (2004). Properties of Ca^{2+}-dependent exocytosis in cultured astrocytes. *Glia*, (46):437–445.

Lavialle, M., Aumann, G., Anlauf, E., Pröls, F., Arpin, M., and Derouiche, A. (2011). Structural plasticity of perisynaptic astrocyte processes involves ezrin and metabotropic glutamate receptors. *Proc. Nat. Acad. Sci. USA*, 108(31):12915–12919.

Lee, C. J., Mannaioni, G., Yuan, H., Woo, D. H., Gingrich, M. B., and Traynelis, S. F. (2007). Astrocytic control of synaptic NMDA receptors. *The Journal of Physiology*, 581(3):1057–1081.

Li, Y. and Rinzel, J. (1994). Equations for $InsP_3$ receptor-mediated $[Ca^{2+}]_i$ oscillations derived from a detailed kinetic model: A Hodgkin-Huxley like formalism. *J. Theor. Biol.*, 166:461–473.

Liu, D., Yang, Q., and Li, S. (2013). Activation of extrasynaptic NMDA receptors induces LTD in rat hippocampal CA1 neurons. *Brain research bulletin*, 93:10–16.

Liu, Q., Xu, Q., Arcuino, G., Kang, J., and Nedergaard, M. (2004a). Astrocyte-mediated activation of neuronal kainate receptors. *Proc. Natl. Acad. Sci. USA*, 101(9):3172–3177.

Liu, Q.-S., Xu, Q., Kang, J., and Nedergaard, M. (2004b). Astrocyte activation of presynaptic metabotropic glutamate receptors modulates hippocampal inhibitory synaptic transmission. *Neuron Glia Biol.*, 1:307–316.

Loebel, A., Silberberg, G., Helbig, D., Markram, H., Tsodyks, M., and Richardson, M. J. E. (2009). Multiquantal release underlies the distribution of synaptic efficacies in the neocortex. *Frontiers in computational neuroscience*, 3.

Losi, G., Mariotti, L., and Carmignoto, G. (2014). GABAergic interneuron to astrocyte signalling: a neglected form of cell communication in the brain. *Phil. Trans. Royal Soc. B: Biological Sciences*, 369(1654):20130609.

Lytton, J., Westlin, M., Burk, S. E., Shull, G. W., and MacLennan, D. H. (1992). Functional comparisons between isoforms of the sarcoplasmic or endoplasmic reticulum of calcium pumps. *J. Biol. Chem.*, 267(20):14483–14489.

Magee, J. (1998). Dendritic hyperpolarization-activated currents modify the integrative properties of hippocampal CA1 pyramidal neurons. *J. Neurosci.*, 18(19):7613–7624.

Magee, J. and Cook, E. (2000). Somatic EPSP amplitude is independent of synapse location in hippocampal pyramidal neurons. *Nat. Neurosci.*, 3:895–903.

Magee, J. C. and Johnston, D. (1997). A synaptically controlled, associative signal for hebbian plasticity in hippocampal neurons. *Science*, 275(5297):209–213.

Magee, J. C. and Johnston, D. (2005). Plasticity of dendritic function. *Current Opinion in Neurobiology*, 15(3):334–342.

Malarkey, E. and Parpura, V. (2011). Temporal characteristics of vesicular fusion in astrocytes: examination of synaptobrevin 2-laden vesicles at single vesicle resolution. *J. Physiol.*, 589(17):4271–4300.

Malenka, R. C. and Bear, M. F. (2004). LTP and LTD: an embarrassment of riches. *Neuron*, 44(1):5–21.

Marchaland, J., Calì, C., Voglmaier, S. M., Li, H., Regazzi, R., Edwards, R. H., and Bezzi, P. (2008). Fast subplasma membrane Ca^{2+} transients control exo-endocytosis of synaptic-like microvesicles in astrocytes. *J. Neurosci.*, 28(37):9122–9132.

Markram, H., Pikus, D., Gupta, A., and Tsodyks, M. (1998a). Potential for multiple mechanisms, phenomena and algorithms for synaptic plasticity at single synapses. *Neuropharmacology*, 37:489–500.

Markram, H., Wang, Y., and Tsodyks, M. (1998b). Differential signaling via the same axon of neocortical pyramidal neurons. *Proc. Natl. Acad. Sci. USA*, 95:5323–5328.

Martín, R., Bajo-Grañeras, R., Moratalla, R., Perea, G., and Araque, A. (2015). Circuit-specific signaling in astrocyte-neuron networks in basal ganglia pathways. *Science*, 349(6249):730–734.

McDermott, C., Hardy, M., Bazan, N., and Magee, J. (2006). Sleep deprivation-induced alterations in excitatory synaptic transmission in the CA1 region of the rat hippocampus. *J. Physiol.*, 570(3):553–565.

McDermott, C., LaHoste, G., Chen, C., Musto, A., Bazan, N., and Magee, J. (2003). Sleep deprivation causes behavioral, synaptic, and membrane excitability alterations in hippocampal neurons. *J. Neurosci.*, 23(29):9687–9695.

Meredith, R. M., Floyer-Lea, A. M., and Paulsen, O. (2003). Maturation of long-term potentiation induction rules in rodent hippocampus: role of GABAergic inhibition. *The Journal of Neuroscience*, 23(35):11142–11146.

Metz, A., Jarsky, T., Martina, M., and Spruston, N. (2005). R-type calcium channels contribute to afterdepolarization and bursting in hippocampal CA1 pyramidal neurons. *J. Neurosci.*, 25(24):5763–5773.

Min, R., Santello, M., and Nevian, T. (2012). The computational power of astrocyte mediated synaptic plasticity. *Front. Comp. Neurosci.*, 6.

Mizuno, T., Kanazawa, I., and Sakurai, M. (2001). Differential induction of LTP and LTD is not determined solely by instantaneous calcium concentration: an essential involvement of a temporal factor. *European Journal of Neuroscience*, 14(4):701–708.

Montana, V., Malarkey, E. B., Verderio, C., Matteoli, M., and Parpura, V. (2006). Vesicular transmitter release from astrocytes. *Glia*, 54:700–715.

Murthy, V. N., Sejnowski, T. J., and Stevens, C. F. (1997). Heterogeneous release properties of visualized individual hippocampal synapses. *Neuron*, 18:599–612.

Naeem, M., McDaid, L., Harkim, J., Wade, J. J., and Marsland, J. (2015). On the role of astroglial syncytia in self-repairing spiking neural networks. *IEEE Trans. Neural Networks and Learning Systems*, page In press.

Navarrete, M. and Araque, A. (2008). Endocannabinoids mediate neuron-astrocyte communication. *Neuron*, 57(6):883–893.

Navarrete, M. and Araque, A. (2010). Endocannabinoids potentiate synaptic transmission through stimulation of astrocytes. *Neuron*, 68(1):113–126.

Navarrete, M., Perea, G., de Sevilla, D., Gómez-Gonzalo, M., Núñez, A., Martín, E., and Araque, A. (2012a). Astrocytes mediate in vivo cholinergic-induced synaptic plasticity. *PLoS Biol.*, 10(2):e1001259.

Navarrete, M., Perea, G., Maglio, L., Pastor, J., García de Sola, R., and Araque, A. (2012b). Astrocyte calcium signal and gliotransmission in human brain tissue. *Cereb. Cortex.*

Nevian, T. and Sakmann, B. (2004). Single spine Ca^{2+} signals evoked by coincident EPSPs and backpropagating action potentials in spiny stellate cells of layer 4 in the juvenile rat somatosensory barrel cortex. *The Journal of Neuroscience*, 24(7):1689–1699.

Nevian, T. and Sakmann, B. (2006). Spine Ca^{2+} signaling in spike-timing-dependent plasticity. *The Journal of Neuroscience*, 26(43):11001–11013.

Ni, Y., Malarkey, E. B., and Parpura, V. (2007). Vesicular release of glutamate mediates bidirectional signaling between astrocytes and neurons. *J. Neurochem.*, 103(4):1273–1284.

Nie, H., Zhang, H., and Weng, H. (2010). Bidirectional neuron–glia interactions triggered by deficiency of glutamate uptake at spinal sensory synapses. *J. Neurophysiol.*, 104(2):713–725.

Nielsen, T. A., DiGregorio, D. A., and Silver, R. A. (2004). Modulation of glutamate mobility reveals the mechanism underlying slow-rising AMPAR EPSCs and the diffusion coefficient in the synaptic cleft. *Neuron*, 42:757–771.

Nimmerjahn, A. (2009). Astrocytes going live: advances and challenges. *J. Physiol.*, 587:1639–1647.

Nimmerjahn, A., Kirchhoff, F., Kerr, J. N. D., and Helmchen, F. (2004). Sulforhodamine 101 as a specific marker of astroglia in the neocortex *in vivo*. *Nat. Methods*, 1:31–37.

Nowak, L., Bregestovski, P., Ascher, P., Herbert, A., and Prochiantz, A. (1984). Magnesium gates glutamate-activated channels in mouse central neurons. *Nature*, 307:462–465.

Oertner, T. G., Sabatini, B. L., Nimchinsky, E. A., and Svoboda, K. (2002). Facilitation at single synapses probed with optical quantal analysis. *Nature Neuroscience*, 5(7):657–664.

Oh, S., Han, K., Park, H., Woo, D. H., Kim, H. Y., Traynelis, S. F., and Lee, C. J. (2012). Protease activated receptor 1-induced glutamate release in cultured astrocytes is mediated by Bestrophin-1 channel but not by vesicular exocytosis. *Mol Brain*, 5(1):38–38.

Okubo, Y., Sekiya, H., Namiki, S., Sakamoto, H., Iinuma, S., Yamasaki, M., Watanabe, M., Hirose, K., and Iino, M. (2010). Imaging extrasynaptic glutamate dynamics in the brain. *Proc. Nat. Acad. Sci. USA*, 107(14):6526–6531.

Otmakhova, N., Otmakhov, N., and Lisman, J. (2002). Pathway-specific properties of AMPA and NMDA-mediated transmission in CA1 hippocampal pyramidal cells. *J. Neurosci.*, 22(4):1199–1207.

Panatier, A., Vallée, J., Haber, M., Murai, K., Lacaille, J., and Robitaille, R. (2011). Astrocytes are endogenous regulators of basal transmission at central synapses. *Cell*, 146:785–798.

Pankratov, Y. and Krishtal, O. (2003). Distinct quantal features of AMPA and NMDA synaptic currents in hippocampal neurons: implication of glutamate spillover and receptor saturation. *Biophys. J.*, 85(5):3375–3387.

Pankratov, Y., Lalo, U., Verkhratsky, A., and North, R. (2007). Quantal release of ATP in mouse cortex. *J. Gen. Physiol.*, 129(3):257–265.

Papouin, T., Ladépêche, L., Ruel, J., Sacchi, S., Labasque, M., Hanini, M., Groc, L., Pollegioni, L., Mothet, J., and Oliet, S. (2012). Synaptic and extrasynaptic NMDA receptors are gated by different endogenous coagonists. *Cell*, 150(3):633–646.

Papouin, T. and Oliet, S. H. R. (2014). Organization, control and function of extrasynaptic NMDA receptors. *Phil. Trans. Royal Soc. B: Biological Sciences*, 369(1654):20130601.

Parpura, V., Grubi˘ sić, V., and Verkhratsky, A. (2011). Ca^{2+} sources for the exocytotic release of glutamate from astrocytes. *Biochim. Biophys. Acta*, 1813(5):984–991.

Parpura, V. and Haydon, P. G. (2000). Physiological astrocytic calcium levels stimulate glutamate release to modulate adjacent neurons. *Proc. Natl. Acad. Sci. USA*, 97(15):8629–8634.

Parpura, V. and Zorec, R. (2010). Gliotransmission: exocytotic release from astrocytes. *Brain Res. Rev.*, 63:83–92.

Parri, H. R., Gould, T. M., and Crunelli, V. (2001). Spontaneous astrocytic Ca^{2+} oscillations in situ drive NMDAR-mediated neuronal excitation. *Nat. Neurosci.*, 4(8):803–812.

Pasti, L., Volterra, A., Pozzan, T., and Carmignoto, G. (1997). Intracellular calcium oscillations in astrocytes: a highly plastic, bidirectional form of communication between neurons and astrocytes *in situ*. *J. Neurosci.*, 17(20):7817–7830.

Perea, G. and Araque, A. (2005). Properties of synaptically evoked astrocyte calcium signal reveal synaptic information processing by astrocyte. *J. Neurosci.*, 25(9):2192–2203.

Perea, G. and Araque, A. (2007). Astrocytes potentiate transmitter release at single hippocampal synapses. *Science*, 317:1083–1086.

Perea, G., Navarrete, M., and Araque, A. (2009). Tripartite synapse: astrocytes process and control synaptic information. *Trends Neurosci.*, 32:421–431.

Perea, G., Yang, A., Boyden, E. S., and Sur, M. (2014). Optogenetic astrocyte activation modulates response selectivity of visual cortex neurons in vivo. *Nature communications*, 5:3262.

Perez-Alvarez, A., Navarrete, M., Covelo, A., Martin, E. D., and Araque, A. (2014). Structural and functional plasticity of astrocyte processes and dendritic spine interactions. *The Journal of Neuroscience*, 34(38):12738–12744.

Petralia, R. S., Wang, Y., Hua, F., Yi, Z., Zhou, A., Ge, L., Stephenson, F. A., and Wenthold, R. J. (2010). Organization of NMDA receptors at extrasynaptic locations. *Neuroscience*, 167(1):68–87.

Pike, F. G., Meredith, R. M., Olding, A. W. A., and Paulsen, O. (1999). Postsynaptic bursting is essential for Hebbian induction of associative long-term potentiation at excitatory synapses in rat hippocampus. *The Journal of Physiology*, 518(2):571–576.

Pinheiro, P. S. and Mulle, C. (2008). Presynaptic glutamate receptors: physiological functions and mechanisms of action. *Nat. Rev. Neurosci.*, 9:423–436.

Pirttimaki, T., Hall, S., and Parri, H. (2011). Sustained neuronal activity generated by glial plasticity. *J. Neurosci.*, 31(21):7637–7647.

Pivneva, T., Haas, B., Reyes-Haro, D., Laube, G., Veh, R., Nolte, C., Skibo, G., and Kettenmann, H. (2008). Store-operated Ca^{2+} entry in astrocytes: different spatial arrangement of endoplasmic reticulum explains functional diversity in vitro and in situ. *Cell Calcium*, 43(6):591–601.

Porto-Pazos, A. B., Veiguela, N., Mesejo, P., Navarrete, M., Alvarellos, A., Ibáñez, O., Pazos, A., and Araque, A. (2011). Artificial astrocytes improve neural network performance. *PloS one*, 6(4):e19109.

Pyle, J. L., Kavalali, E. T., Piedras-Rentería, E. S., and Tsien, R. W. (2000). Rapid reuse of readily releasable pool vesicles at hippocampal synapses. *Neuron*, 28:221–231.

Python Software Foundation (2015). Python language reference, version 2.7.

Raghavachari, S. and Lisman, J. E. (2004). Properties of quantal transmission at CA1 synapses. *J. Neurophysiol.*, 92:2456–2467.

Rauch, A., La Camera, G., Lüscher, H., Senn, W., and Fusi, S. (2003). Neocortical pyramidal cells respond as integrate-and-fire neurons to in vivo–like input currents. *Journal of Neurophysiology*, 90(3):1598–1612.

Rebecchi, M. J. and Pentyala, S. N. (2000). Structure, function, and control of phosphoinositide-specific phospholipase C. *Physiol. Rev.*, 80(4):1291–1335.

Regehr, W. F., Delaney, K. R., and Tank, D. W. (1994). The role of presynaptic calcium in short-term enhancement at the hippocampal mossy fiber synapse. *J. Neurosci.*, 14:523–537.

Reyes-Haro, D., Müller, J., Boresch, M., Pivneva, T., Benedetti, B., Scheller, A., Nolte, C., and Kettenmann, H. (2010). Neuron–astrocyte interactions in the medial nucleus of the trapezoid body. *The Journal of General Physiology*, 135(6):583–594.

Routh, B., Johnston, D., Harris, K., and Chitwood, R. (2009). Anatomical and electrophysiological comparison of CA1 pyramidal neurons of the rat and mouse. *J. Neurophysiol.*, 102(4):2288–2302.

Rusakov, D. A. and Kullmann, D. M. (1998). Extrasynaptic glutamate diffusion in the hippocampus: ultrastructural constraints, uptake, and receptor activation. *J. Neurosci.*, 18(9):3158–3170.

Rusakov, D. A., Scimemi, A., Walker, M. C., and Kullmann, D. M. (2004). Comment on "Role of NMDA Receptor Subtypes in Governing the Direction of Hippocampal Synaptic Plasticity". *Science*, 305:1912.

Sahlender, D. A., Savtchouk, I., and Volterra, A. (2014). What do we know about gliotransmitter release from astrocytes? *Phil. Tran. R. Soc. B*, 369:20130592.

Santello, M., Bezzi, P., and Volterra, A. (2011). TNFα controls glutamatergic gliotransmission in the hippocampal dentate gyrus. *Neuron*, 69:988–1001.

Santello, M. and Volterra, A. (2009). Synaptic modulation by astrocytes via Ca^{2+}-dependent glutamate release. *Neuroscience*, 158(1):253–259.

Schikorski, T. and Stevens, C. F. (1997). Quantitative ultrastructural analysis of hippocampal excitatory synapses. *J. Neurosci.*, 17(15):5858–5867.

Serrano, A., Haddjeri, N., Lacaille, J., and Robitaille, R. (2006). GABAergic network activation of glial cells underlies heterosynaptic depression. *J. Neurosci.*, 26(20):5370–5382.

Shigetomi, E., Bowser, D. N., Sofroniew, M. V., and Khakh, B. S. (2008). Two forms of astrocyte calcium excitability have distinct effects on NMDA receptor-mediated slow inward currents in pyramidal neurons. *J. Neurosci.*, 28(26):6659–6663.

Shouval, H., Bear, M., and Cooper, L. (2002). A unified model of NMDA receptor-dependent bidirectional synaptic plasticity. *Proc. Natl. Acad. Sci. USA*, 99(16):10831–10836.

Shulz, D. E. and Jacob, V. (2010). Spike-timing-dependent plasticity in the intact brain: counteracting spurious spike coincidences. *Frontiers in Synaptic Neuroscience*, 2.

Sims, C. E. and Allbritton, N. L. (1998). Metabolism of inositol 1,4,5-trisphosphate and inositol 1,3,4,5-tetrakisphosphate by the oocytes of *Xenopus laevis*. *J. Biol. Chem.*, 273(7):4052–4058.

Sjöström, P. J. and Nelson, S. B. (2002). Spike timing, calcium signals and synaptic plasticity. *Current Opinion in Neurobiology*, 12(3):305–314.

Sjöström, P. J., Rancz, E. A., Roth, A., and Häusser, M. (2008). Dendritic excitability and synaptic plasticity. *Physiological Reviews*, 88(2):769–840.

Smith, M., Ellis-Davies, G., and Magee, J. (2003). Mechanism of the distance-dependent scaling of Schaffer collateral synapses in rat CA1 pyramidal neurons. *J. Physiol.*, 548(1):245–258.

Spruston, N., Jonas, P., and Sakmann, B. (1995). Dendritic glutamate receptor channels in rat hippocampal CA3 and CA1 pyramidal neurons. *J. Physiol.*, 482(2):325–352.

Stevens, C. F. and Wang, Y. (1995). Facilitation and depression at single central synapses. *Neuron*, 14:795–802.

Stimberg, M., Goodman, D. F. M., Benichoux, V., and Brette, R. (2014). Equation-oriented specification of neural models for simulations. *Frontiers in Neuroinformatics*, 8.

Südhof, T. C. (2004). The synaptic vesicle cycle. *Annu. Rev. Neurosci.*, 27:509–547.

Sun, W., McConnell, E., Pare, J.-F., Xu, Q., Chen, M., Peng, W., Lovatt, D., Han, X., Smith, Y., and Nedergaard, M. (2013). Glutamate-dependent neuroglial calcium signaling differs between young and adult brain. *Science*, 339(6116):197–200.

Tian, G.-F., Azmi, H., Takahiro, T., Xu, Q., Peng, W., Lin, J., Oberheim, N., Lou, N., Zielke, H. R., and Nedergaard, M. (2005). An astrocytic basis of epilepsy. *Nature Med.*, 11(9):973–981.

Traynelis, S., Wollmuth, L., McBain, C., Menniti, F., Vance, K., Ogden, K., Hansen, K., Yuan, H., Myers, S., and Dingledine, R. (2010). Glutamate receptor ion channels: structure, regulation, and function. *Pharmacol. Rev.*, 62(3):405–496.

Tsodyks, M. (2005). Activity-dependent transmission in neocortical synapses. In Chow, C. C., Gutkin, B., D., H., C., M., and Dalibard, J., editors, *Methods and Models in Neurophysics*, pages 245–265. Elsevier.

Tsodyks, M. V. and Markram, H. (1997). The neural code between neocortical pyramidal neurons depends on neurotransmitter release probability. *Proc. Natl. Acad. Sci. USA*, 94:719–723.

Valtorta, F., Meldolesi, J., and Fesce, R. (2001). Synaptic vesicles: is kissing a matter of competence? *Trends Cell. Biol.*, 11:324–328.

Vandecaetsbeek, I., Trekels, M., De Maeyer, M., Ceulemans, H., Lescrinier, E., Raeymaekers, L., Wuytack, F., and Vangheluwe, P. (2009). Structural basis for the high Ca^{2+} affinity of the ubiquitous SERCA2b Ca^{2+} pump. *Proc. Nat. Acad. Sci. USA*, 106(44):18533–18538.

Ventura, R. and Harris, K. M. (1999). Three-dimensional relationships between hippocampal synapses and astrocytes. *J. Neurosci.*, 19(16):6897–6906.

Volterra, A., Liaudet, N., and Savtchouk, I. (2014). Astrocyte Ca^{2+} signalling: an unexpected complexity. *Nature Reviews Neuroscience*, 15:327–334.

Volterra, A. and Meldolesi, J. (2005). Astrocytes, from brain glue to communication elements: the revolution continues. *Nat. Rev. Neurosci.*, 6(8):626–640.

Wade, J. J., McDaid, L. J., Harkin, J., Crunelli, V., and Kelso, J. A. S. (2011). Bidirectional coupling between astrocytes and neurons mediates learning and dynamic coordination in the brain: a multiple modeling approach. *PLoS One*, 6(12):e29445.

Wallach, G., Lallouette, J., Herzog, N., De Pittà, M., Ben-Jacob, E., Berry, H., and Hanein, Y. (2014). Glutamate-mediated astrocytic filfilter of neuronal activity. *PLoS Comput. Biol.*, 10(12):e1003964.

Wang, X., Lou, N., Xu, Q., Tian, G.-F., Peng, W. G., Han, X., Kang, J., Takano, T., and Nedergaard, M. (2006). Astrocytic Ca^{2+} signaling evoked by sensory stimulation *in vivo*. *Nat. Neurosci.*, 9(6):816–823.

Wittenberg, G. M. and Wang, S. S.-H. (2006). Malleability of spike-timing-dependent plasticity at the CA3–CA1 synapse. *The Journal of Neuroscience*, 26(24):6610–6617.

Woo, D. H., Han, K., Shim, J. W., Yoon, B., Kim, E., Bae, J. Y., Oh, S., Hwang, E. M., Marmorstein, A. D., Bae, Y. C., Park, J., and Lee, C. J. (2012). TREK-1 and Best1 channels mediate fast and slow glutamate release in astrocytes upon GPCR activation. *Cell*, 151(1):25–40.

Zhang, B.-X., Zhao, H., and Muallem, S. (1993). Calcium dependent kinase and phosphatase control inositol-1,4,5-trisphopshate-mediated calcium release: modification by agonist stimulation. *J. Biol. Chem.*, 268(5):10997–11001.

Zorec, R., Araque, A., Carmignoto, G., Haydon, P., Verkhratsky, A., and Parpura, V. (2012). Astroglial excitability and gliotransmission: An appraisal of Ca^{2+} as a signaling route. *ASN Neuro*, 4(2):e00080.

Zucker, R. S. and Regehr, W. G. (2002). Short-term synaptic plasticity. *Annu. Rev. Physiol.*, 64:355–405.